

Generalized implementation of the order-preserving mapping for mapped WENO schemes

Ruo Li^a, Wei Zhong^{b,c,*}

^aCAPT, LMAM and School of Mathematical Sciences, Peking University, Beijing 100871, China

^bSchool of Mathematical Sciences, Peking University, Beijing 100871, China

^cNorthwest Institute of Nuclear Technology, Xi'an 710024, China

Abstract

A serious and ubiquitous issue in existing mapped WENO schemes is that most of them can hardly preserve high resolutions and in the meantime prevent spurious oscillations on solving hyperbolic conservation laws with long output times. Our goal in this article is to address this widely concerned problem [3, 4, 15, 29, 16, 18]. We firstly take a closer look at the mappings of various existing mapped WENO schemes and devise a general formula for them. It helps us to extend the *order-preserving* (*OP*) criterion, originally defined and carefully examined in [18], into the design of the mappings. Next, we propose the implementation of obtaining the new mappings satisfying the *OP* criterion from those of the existing mapped WENO-X schemes where the notation “X” is used to identify the version of the existing mapped WENO scheme, e.g., X = M [11], PM6 [3], or PPM5 [15], et al. Then we build the resultant mapped WENO schemes and denote them as MOP-WENO-X. The numerical solutions of the one-dimensional linear advection equation with different initial conditions and some standard numerical experiments of two-dimensional Euler system, computed by the MOP-WENO-X schemes, are compared with the ones generated by their corresponding WENO-X schemes and the WENO-JS scheme. To summarize, the MOP-WENO-X schemes gain definite advantages in terms of attaining high resolutions and meanwhile avoiding spurious oscillations near discontinuities for long output time simulations of the one-dimensional linear advection problems, as well as significantly reducing the post-shock oscillations in the simulations of the two-dimensional steady problems with strong shock waves.

Keywords: Mapped WENO, Order-preserving mapping, Hyperbolic conservation laws

1. Introduction

The essentially non-oscillatory (ENO) schemes [8, 9, 10, 7] and the weighted ENO (WENO) schemes [26, 27, 19, 13, 25] have developed quite successfully in recent decades to solve the hyperbolic conservation problems, especially those may generate discontinuities and smooth small-scale structures as time evolves in its solution even if the initial condition is smooth. The main purpose of this paper is to find a general method to introduce the *order-preserving* (*OP*) mapping proposed in our previous work [18] for improving the existing mapped WENO schemes for the approximation of the hyperbolic conservation laws in the form

$$\frac{\partial \mathbf{u}}{\partial t} + \nabla \cdot \mathbf{F}(\mathbf{u}) = 0, \quad (1)$$

where $\mathbf{u} = (u_1, \dots, u_m) \in \mathbb{R}^m$ is the vector of the conserved variables and $\mathbf{F}(\mathbf{u})$ is the vector of the Cartesian components of flux.

Harten et al. [8] introduced the ENO schemes. They used the smoothest stencil from r possible candidate stencils based on the local smoothness to perform a polynomial reconstruction such that it yields high-order accuracy in

*Corresponding author

Email addresses: rli@math.pku.edu.cn (Ruo Li), zhongwei2016@pku.edu.cn (Wei Zhong)

smooth regions but avoids spurious oscillations at or near discontinuities. Liu, Osher, and Chan [19] introduced the first WENO scheme, an improved version of the ENO methodology with a cell-averaged approach, by using a nonlinear convex combination of all the candidate stencils to achieve a higher order of accuracy than the ENO schemes while retain the essential non-oscillatory property at or near discontinuities. In other words, it achieves $(r + 1)$ th-order of accuracy from the r th-order ENO schemes [8, 9, 10] in the smooth regions while behaves similarly to the r th-order ENO schemes in regions including discontinuities. In [13], Jiang and Shu proposed the classic WENO-JS scheme with a new measurement of the smoothness of the numerical solutions on substencils (hereafter, denoted by smoothness indicator), by using the sum of the normalized squares of the scaled L_2 -norms of all the derivatives of r local interpolating polynomials, to obtain $(2r - 1)$ th-order of accuracy from the r th-order ENO schemes.

The WENO-JS scheme has become a very popular and quite successful methodology for solving compressible flows modeled by means of hyperbolic conservation laws in the form of Eq.(1). However, it was less than fifth-order for many cases such as at or near critical points of order $n_{cp} = 1$ in the smooth regions. Here, we refer to n_{cp} as the order of the critical point; e.g., $n_{cp} = 1$ corresponds to $f' = 0, f'' \neq 0$ and $n_{cp} = 2$ corresponds to $f' = 0, f'' = 0, f''' \neq 0$, etc. In particular, Henrick et al. [11] identified that the fifth-order WENO-JS scheme fails to yield the optimal convergence order at or near critical points where the first derivative vanishes but the third order derivative does not simultaneously. Then, in the same article, they derived the necessary and sufficient conditions on the nonlinear weights for optimality of the convergence rate of the fifth-order WENO schemes and these conditions were reduced to a simpler sufficient condition [1] which could be easily extended to the $(2r - 1)$ th-order WENO schemes [4]. Moreover, also in [11], Henrick et al. devised the original mapped WENO scheme, named WENO-M hereafter, by constructing a mapping function which satisfies the sufficient condition to achieve the optimal order of accuracy.

Later, following the idea of incorporating a mapping procedure to maintain the nonlinear weights of the convex combination of stencils as near as possible to the ideal weights of optimal order accuracy, various versions of mapped WENO schemes have been successfully proposed. In [4], Feng et al. rewrote the mapping function of the WENO-M scheme in a simple and more meaningful form, and then extended it to a general class of improved mapping functions leading to the family of the WENO-IM(k, A) schemes, where k is a positive even integer and A a positive real number. It was indicated that by taking $k = 2$ and $A = 0.1$ in the WENO-IM(k, A) scheme, far better numerical solutions with less dissipation and higher resolution could be obtained than that of the WENO-M scheme. Unfortunately, the numerical experiments in [29] showed that the seventh- and ninth- order WENO-IM(2, 0.1) schemes generated evident spurious oscillations near discontinuities when the output time is large. In addition, our numerical experiments as shown in Fig. 5, Fig. 8 and Fig. 9 of this paper indicate that, even for the fifth-order WENO-IM(2, 0.1) scheme, the spurious oscillations are also produced when the grid number increases or a different initial condition is used. Recently, Feng et al. [3] pointed out that, when the WENO-M scheme was used for solving the problems with discontinuities for long output times, its mapping function may amplify the effect from the non-smooth stencils leading to a potential loss of accuracy near discontinuities. To amend this drawback, a piecewise polynomial mapping function with two additional requirements, that is, $g'(0) = 0$ and $g'(1) = 0$ ($g(x)$ denotes the mapping function), to the original criteria in [11] was proposed. The recommended WENO-PM6 scheme [3] achieved significantly higher resolution than the WENO-M scheme when computing the one-dimensional linear advection problem with long output times. However, it may generate the spurious oscillations near the discontinuities as shown in Fig. 8 of [4] and Figs. 3-8 of [29].

Many other mapped WENO schemes, such as the WENO-PPM n [15], WENO-RM($mn0$) [29], WENO-MAIM i [16], WENO-ACM [17] schemes and et al., have been successfully developed to enhance the performances of the classic WENO-JS scheme in some ways, like achieving optimal convergence orders near critical points in smooth regions, having lower numerical dissipations, achieving higher resolutions near discontinuities, or reducing the computational costs, and we refer to the references for more details. However, as mentioned in previously published literatures [4, 29], most of the existing improved mapped WENO schemes could not prevent the spurious oscillations near discontinuities, especially for long output time simulations. Moreover, when simulating the two-dimensional steady problems with strong shock waves, the post-shock oscillations, which were systematically studied for WENO schemes by Zhang et al. [31], become very severe in the solutions of most of the existing improved mapped WENO schemes [17].

In the previous work of this paper [18], the authors made a further study of the nonlinear weights of the existing mapped WENO schemes, by taking the ones developed in [3, 4, 16, 18] as examples. It was found that the order of the nonlinear weights for the substencils of the same global stencil has been changed at many points in the mapping

process of all these considered mapped WENO schemes. The order-change of the nonlinear weights is caused by weights increasing of non-smooth substencils and weights decreasing of smooth substencils. It was revealed that this is the essential cause of the potential loss of accuracy of the WENO-M scheme and the spurious oscillation generation of the existing improved mapped WENO schemes, through theoretical analysis and extensive numerical tests. In the same article, the definition of the *order-preserving (OP)* mapping was given and suggested as an additional criterion in the design of the mapping function. Then a new mapped WENO scheme with its mapping function satisfying the additional criterion was proposed. Extensive numerical experiments showed that this scheme can achieve the optimal convergence order of accuracy even at critical points. It also can decrease the numerical dissipations and obtain high resolution but do not generate spurious oscillation near discontinuities even if the output time is large. Moreover, it was observed clearly that it exhibits significant advantage in reducing the post-shock oscillations when calculating the steady problems with strong shock waves in two dimension.

In this article, the idea of introducing the *OP* criterion into the design of the mapping functions proposed in [18] is extended to various existing mapped WENO schemes. In fact, a general formula for the mapping functions of various existing mapped WENO schemes is obtained that allows the extension of the *OP* criterion to all existing mapped WENO schemes. The notation MOP-WENO-X is used to denote the improved mapped WENO scheme considering the *OP* criterion based on the existing WENO-X scheme. A new function named **minDist** is defined (see Definition 3 in subsection 3.3 below). A general algorithm to construct *OP* mappings through the existing mapping functions by using the **minDist** function is proposed. Extensive numerical tests are conducted to demonstrate the performances of the MOP-WENO-X schemes: (1) a series of accuracy tests shows the capacity of the MOP-WENO-X schemes to achieve the optimal convergence order in smooth regions with first-order critical points and their advantages in long output time simulations of the problems with very high-order critical points; (2) the one-dimensional linear advection equation with two kinds of initial conditions for long output times are then presented to demonstrate that the MOP-WENO-X schemes can obtain high resolution and meanwhile avoid spurious oscillation near discontinuities; (3) some benchmark tests of steady problems with strong shock waves modeled via the two dimensional Euler equations are computed, it is clear that the MOP-WENO-X schemes also enjoy significant advantage in reducing the post-shock oscillations.

The remainder of this paper is organized as follows. In Section 2, we briefly review the preliminaries to understand the finite volume method and the procedures of the WENO-JS [13], WENO-M [11] and other versions of mapped WENO schemes. Section 3 presents a general method to introduce the *OP* mapping for improving the existing mapped WENO schemes. Some numerical results are provided in Section 4 to illustrate advantages of the proposed WENO schemes. Finally, concluding remarks are given in Section 5 to close this paper.

2. Brief review of the WENO schemes

For simplicity of presentation but without loss of generality, we devote our discussion to the following one-dimensional linear hyperbolic conservation equation

$$\frac{\partial u}{\partial t} + \frac{\partial f(u)}{\partial x} = 0, \quad x_l < x < x_r, t > 0, \quad (2)$$

with the initial condition $u(x, 0) = u_0(x)$. We only confine our attention to the uniform meshes in this paper and the WENO method with non-uniform meshes can refer to [28, 12]. Throughout this paper, we assume that the given domain $[x_l, x_r]$ is discretized into the set of uniform cells $I_j := [x_{j-1/2}, x_{j+1/2}]$, $j = 1, \dots, N$ with the cell size $\Delta x = \frac{x_r - x_l}{N}$. The associated cell centers and cell boundaries are denoted by $x_j = x_l + (j - 1/2)\Delta x$ and $x_{j\pm 1/2} = x_j \pm \Delta x/2$, respectively. The notation $\bar{u}(x_j, t) = \frac{1}{\Delta x} \int_{x_{j-1/2}}^{x_{j+1/2}} u(\xi, t) d\xi$ indicates the cell average of I_j . The one-dimensional linear hyperbolic conservation equation in Eq.(2) can be approximated by a system of ordinary differential equations, yielding the semi-discrete finite volume form:

$$\begin{aligned} \frac{d\bar{u}_j(t)}{dt} &\approx \mathcal{L}(u_j), \\ \mathcal{L}(u_j) &= -\frac{1}{\Delta x} (\hat{f}_{j+1/2} - \hat{f}_{j-1/2}), \end{aligned} \quad (3)$$

where $\bar{u}_j(t)$ is the numerical approximation to the cell average $\bar{u}(x_j, t)$, and the numerical flux $\hat{f}_{j\pm 1/2}$ is a replacement of the physical flux function $f(u)$ at the cell boundaries $x_{j\pm 1/2}$ and it is defined by $\hat{f}_{j\pm 1/2} = \hat{f}(u_{j\pm 1/2}^-, u_{j\pm 1/2}^+)$. The notations $u_{j\pm 1/2}^\pm$ refer to the limits of u and their values of $u_{j\pm 1/2}^\pm$ can be obtained by the technique of reconstruction, like the WENO reconstruction procedures narrated latter. In this paper, we choose the global Lax-Friedrichs flux

$$\hat{f}(a, b) = \frac{1}{2}[f(a) + f(b) - \alpha(b - a)],$$

where $\alpha = \max_u |f'(u)|$ is a constant and the maximum is taken over the whole range of u .

2.1. The WENO-JS reconstruction

Firstly, we review the process of the classic fifth-order WENO-JS reconstruction [13]. For brevity, we describe only the reconstruction procedure of the left-biased $u_{j+1/2}^-$, and the right-biased one $u_{j+1/2}^+$ can trivially be computed by mirror symmetry with respect to the location $x_{j+1/2}$ of $u_{j+1/2}^-$. We drop the subscript “-” below just for simplicity of notation.

To construct the values of $u_{j+1/2}$ from known cell average values \bar{u}_j , a 5-point global stencil $S^5 = \{I_{j-2}, I_{j-1}, I_j, I_{j+1}, I_{j+2}\}$ is used in the fifth-order WENO-JS scheme. It is subdivided into three 3-point substencils $S_s = \{I_{j+s-2}, I_{j+s-1}, I_{j+s}\}$ with $s = 0, 1, 2$. It is known that the third-order approximations of $u(x_{j+1/2}, t)$ associated with these substencils are explicitly given by

$$\begin{aligned} u_{j+1/2}^0 &= \frac{1}{6}(2\bar{u}_{j-2} - 7\bar{u}_{j-1} + 11\bar{u}_j), \\ u_{j+1/2}^1 &= \frac{1}{6}(-\bar{u}_{j-1} + 5\bar{u}_j + 2\bar{u}_{j+1}), \\ u_{j+1/2}^2 &= \frac{1}{6}(2\bar{u}_j + 5\bar{u}_{j+1} - \bar{u}_{j+2}). \end{aligned} \quad (4)$$

Then the $u_{j+1/2}$ of global stencil S^5 is computed by a weighted average of those third-order approximations of substencils, taking the form

$$u_{j+1/2} = \sum_{s=0}^2 \omega_s u_{j+1/2}^s. \quad (5)$$

The nonlinear weights ω_s in the classic WENO-JS scheme is defined as

$$\omega_s^{\text{JS}} = \frac{\alpha_s^{\text{JS}}}{\sum_{l=0}^2 \alpha_l^{\text{JS}}}, \alpha_s^{\text{JS}} = \frac{d_s}{(\epsilon + \beta_s)^2}, \quad s = 0, 1, 2, \quad (6)$$

where d_0, d_1, d_2 are called the ideal weights of ω_s since they generate the central upstream fifth-order scheme for the global stencil S^5 . It is known that $d_0 = 0.1, d_1 = 0.6, d_2 = 0.3$ and in smooth regions we can get $\sum_{s=0}^2 d_s u_{j+1/2}^s = u(x_{j+1/2}, t) + O(\Delta x^5)$. ϵ is a small positive number introduced to prevent the denominator becoming zero. The parameters β_s are the smoothness indicators for the third-order approximations $u_{j+1/2}^s$ and their explicit formulas can be obtained from [13], taking the form

$$\begin{aligned} \beta_0 &= \frac{13}{12}(\bar{u}_{j-2} - 2\bar{u}_{j-1} + \bar{u}_j)^2 + \frac{1}{4}(\bar{u}_{j-2} - 4\bar{u}_{j-1} + 3\bar{u}_j)^2, \\ \beta_1 &= \frac{13}{12}(\bar{u}_{j-1} - 2\bar{u}_j + \bar{u}_{j+1})^2 + \frac{1}{4}(\bar{u}_{j-1} - \bar{u}_{j+1})^2, \\ \beta_2 &= \frac{13}{12}(\bar{u}_j - 2\bar{u}_{j+1} + \bar{u}_{j+2})^2 + \frac{1}{4}(3\bar{u}_j - 4\bar{u}_{j+1} + \bar{u}_{j+2})^2. \end{aligned}$$

In general, the fifth-order WENO-JS scheme is able to recover optimal convergence rate of accuracy in smooth regions. However, when at or near critical points where the first derivative vanishes but the third derivative does not simultaneously, it loses accuracy and its convergence rate of accuracy decreases to third-order or even less. We refer to [11] for more details.

2.2. The mapped WENO reconstructions

To address the issue of the WENO-JS scheme mentioned above, Henrick et al. [11] made a systematic truncation error analysis of Eq.(3) in its corresponding finite difference version by using the Taylor series expansions of the Eq. (4), and hence they derived the necessary and sufficient conditions on the weights for the fifth-order WENO scheme to achieve the formal fifth-order of convergence at smooth regions of the solution, taking the form

$$\sum_{s=0}^2 (\omega_s^\pm - d_s) = O(\Delta x^6), \quad \sum_{s=0}^2 A_s (\omega_s^+ - \omega_s^-) = O(\Delta x^3), \quad \omega_s^\pm - d_s = O(\Delta x^2), \quad (7)$$

where the superscripts “+” and “-” on ω_s correspond to their use in either $u_{j+1/2}^s$ and $u_{j-1/2}^s$ stencils respectively. Since the first equation in Eq.(7) always holds due to the normalization, a simpler sufficient condition for the fifth-order convergence is given as [1]

$$\omega_s^\pm - d_s = O(\Delta x^3), \quad s = 0, 1, 2. \quad (8)$$

The conditions Eq.(7) or Eq.(8) may not hold in the case of smooth extrema or at critical points when the fifth-order WENO-JS scheme is used. An innovative idea of fixing this deficiency, originally proposed by Henrick in [11], is to design a mapping function to make ω_s approximating the ideal weights d_s at critical points to the required third order $O(\Delta x^3)$. The first mapping function devised by Henrick et al. in [11] is given as

$$(g^M)_s(\omega) = \frac{\omega(d_s + d_s^2 - 3d_s\omega + \omega^2)}{d_s^2 + (1 - 2d_s)\omega}, \quad s = 0, 1, 2. \quad (9)$$

We can verify that $(g^M)_s(\omega)$ meets the conditions in Eq.(8) as it is a non-decreasing monotone function on $[0, 1]$ with finite slopes and satisfies the following properties.

Lemma 1. *The mapping function $(g^M)_s(\omega)$ defined by Eq.(9) satisfies:*

- C1. $0 \leq (g^M)_s(\omega) \leq 1, (g^M)_s(0) = 0, (g^M)_s(1) = 1;$
- C2. $(g^M)_s(d_s) = d_s;$
- C3. $(g^M)'_s(d_s) = (g^M)''_s(d_s) = 0.$

Following Henrick’s idea, a great many improved mapping functions were successfully proposed [4, 3, 15, 29, 16, 17, 18]. To clarify our major concern and provide convenience to readers while for brevity in description, we only state some mapping functions in the following context, and we refer to references for properties similar to Lemma 1 and more details of these mapping functions.

■ WENO-IM(k, A) [4]

$$(g^{\text{IM}})_s(\omega; k, A) = d_s + \frac{(\omega - d_s)^{k+1} A}{(\omega - d_s)^k A + \omega(1 - \omega)}, \quad A > 0, k = 2n, n \in \mathbb{N}^+. \quad (10)$$

■ WENO-PM k [3]

$$(g^{\text{PM}})_s(\omega) = c_1(\omega - d_s)^{k+1}(\omega + c_2) + d_s, \quad k \geq 2, \quad (11)$$

where c_1, c_2 are constants with specified parameters k and d_s , taking the following forms

$$c_1 = \begin{cases} (-1)^k \frac{k+1}{d_s^{k+1}}, & 0 \leq \omega \leq d_s, \\ -\frac{k+1}{(1-d_s)^{k+1}}, & d_s < \omega \leq 1, \end{cases} \quad c_2 = \begin{cases} \frac{d_s}{k+1}, & 0 \leq \omega \leq d_s, \\ \frac{d_s - (k+2)}{k+1}, & d_s < \omega \leq 1. \end{cases}$$

■ WENO-PPM n [15]

$$(g_s^{\text{PPM}n})_s(\omega) = \begin{cases} (g_{s,L}^{\text{PPM}n})_s(\omega), & \omega \in [0, d_s] \\ (g_{s,R}^{\text{PPM}n})_s(\omega), & \omega \in (d_s, 1], \end{cases} \quad (12)$$

and for $n = 5$,

$$(g_{s,L}^{\text{PPM5}})_s(\omega) = d_s(1 + (a - 1)^5), \quad (g_{s,R}^{\text{PPM5}})_s(\omega) = d_s + b^4(\omega - d_s)^5. \quad (13)$$

where $a = \omega/d_s, b = 1/(d_s - 1)$.

■ WENO-RM(mn) [29]

$$(g^{\text{RM}})_s(\omega) = d_s + \frac{(\omega - d_s)^{n+1}}{a_0 + a_1\omega + \cdots + a_{m+1}\omega^{m+1}}, \quad m \leq n \leq 8, \quad (14)$$

where

$$\begin{cases} a_i = C_{n+1}^i (-d_s)^{n-i}, & i = 0, 1, \dots, m, \\ a_{m+1} = (1 - d_s)^n - \sum_{i=0}^m a_i. \end{cases} \quad (15)$$

And $m = 2, n = 6$ is recommended in [29], then

$$(g^{\text{RM}})_s(\omega) = d_s + \frac{(\omega - d_s)^7}{a_0 + a_1\omega + a_2\omega^2 + a_3\omega^3}, \quad \omega \in [0, 1] \quad (16)$$

where

$$a_0 = d_s^6, \quad a_1 = -7d_s^5, \quad a_2 = 21d_s^4, \quad a_3 = (1 - d_s)^6 - \sum_{i=0}^2 a_i. \quad (17)$$

■ WENO-MAIM1 [16]

$$(g^{\text{MAIM1}})_s(\omega) = d_s + \frac{A \left(\frac{1+(-1)^k}{2} + \frac{1+(-1)^{k+1}}{2} \cdot \text{sgm}(\omega - d_s, \delta, 1, k) \right) \cdot (\omega - d_s)^{k+1}}{A \left(\frac{1+(-1)^k}{2} + \frac{1+(-1)^{k+1}}{2} \cdot \text{sgm}(\omega - d_s, \delta, 1, k) \right) \cdot (\omega - d_s)^k + \omega^{\frac{d_s}{m_s \omega + \epsilon_A}} (1 - \omega)^{\frac{1-d_s}{m_s(1-\omega) + \epsilon_A}}}, \quad (18)$$

with

$$\text{sgm}(x, \delta, B, k) = \begin{cases} \frac{x}{|x|}, & |x| \geq \delta, \\ \frac{x}{(B(\delta^2 - x^2))^{k+3} + |x|}, & |x| < \delta. \end{cases} \quad (19)$$

In Eq.(18), $k \in \mathbb{N}^+, A > 0, \delta > 0$ with $\delta \rightarrow 0, \epsilon_A$ is a very small positive number to prevent the denominator becoming zero, and $m_s \in \left[\frac{\alpha_s}{k+1}, M \right)$ with M being a finite positive constant real number and α_s a positive constant that only depends on s in the fifth-order WENO-MAIM1 scheme. In Eq.(19), the positive parameter B is a scale transformation factor introduced to adjust the shape of the mapping function and it is set to be 1 in WENO-MAIM1 while to be other values in the following WENO-ACM schemes.

■ WENO-ACM [17]

$$(g^{\text{ACM}})_s(\omega) = \begin{cases} \frac{d_s}{2} \text{sgm}(\omega - \text{CFS}_s, \delta_s, B, k) + \frac{d_s}{2}, & \omega \leq d_s, \\ \frac{1 - d_s}{2} \text{sgm}(\omega - \overline{\text{CFS}}_s, \delta_s, B, k) + \frac{1 + d_s}{2}, & \omega > d_s, \end{cases} \quad (20)$$

where $\text{CFS}_s \in (0, d_s), \overline{\text{CFS}}_s = 1 - \frac{1-d_s}{d_s} \times \text{CFS}_s$ with $\overline{\text{CFS}}_s \in (d_s, 1)$, and $\delta_s < \min \left\{ \text{CFS}_s, d_s - \text{CFS}_s, (1 - d_s) \left(1 - \frac{\text{CFS}_s}{d_s} \right), \frac{1-d_s}{d_s} \text{CFS}_s \right\}$.

■ MIP-WENO-ACM k [18]

$$(g^{\text{MIP-ACM}k})_s(\omega) = \begin{cases} k_s \omega, & \omega \in [0, \text{CFS}_s), \\ d_s, & \omega \in [\text{CFS}_s, \overline{\text{CFS}}_s], \\ 1 - k_s(1 - \omega), & \omega \in (\overline{\text{CFS}}_s, 1], \end{cases} \quad (21)$$

where $\text{CFS}_s \in (0, d_s)$, $\overline{\text{CFS}}_s = 1 - \frac{1-d_s}{d_s} \times \text{CFS}_s$ with $\overline{\text{CFS}}_s \in (d_s, 1)$, and $k_s \in \left[0, \frac{d_s}{\text{CFS}_s}\right]$.

By using the mapping function $(g^X)_s(\omega)$, where the superscript ‘‘X’’ correspond to ‘‘M’’, ‘‘PM6’’, ‘‘IM’’, etc., the nonlinear weights of the associated WENO-X scheme are defined as

$$\omega_s^X = \frac{\alpha_s^X}{\sum_{l=0}^2 \alpha_l^X}, \alpha_s^X = (g^X)_s(\omega_s^{\text{JS}}), \quad s = 0, 1, 2,$$

where ω_s^{JS} are calculated by Eq.(6).

In references, it has been analyzed and proved in detail that the WENO-X schemes can retain the optimal order of accuracy in smooth regions even at or near critical points.

3. A general method to introduce order-preserving mapping for mapped WENO schemes

3.1. The order-preserving mapping

To maintain coherence and for the convenience of the readers, we state the definition of *order-preserving/non-order-preserving* mapping and *OP/non-OP* point proposed in [18].

Definition 1. (*order-preserving/non-order-preserving mapping*) Suppose that $(g^X)_s(\omega)$, $s = 0, \dots, r-1$ is a monotone increasing piecewise mapping function of the $(2r-1)$ th-order mapped WENO-X scheme. If for $\forall m, n \in \{0, \dots, r-1\}$, when $\omega_m > \omega_n$, we have

$$(g^X)_m(\omega_m) \geq (g^X)_n(\omega_n). \quad (22)$$

and when $\omega_m = \omega_n$, we have $(g^X)_m(\omega_m) = (g^X)_n(\omega_n)$, then we say the set of mapping functions $\{(g^X)_s(\omega), s = 0, \dots, r-1\}$ is **order-preserving (OP)**. Otherwise, we say the set of mapping functions $\{(g^X)_s(\omega), s = 0, \dots, r-1\}$ is **non-order-preserving (non-OP)**.

Definition 2. (*OP/non-OP point*) Let S^{2r-1} denote the $(2r-1)$ -point global stencil centered around x_j . Assume that S^{2r-1} is subdivided into r -point substencils $\{S_0, \dots, S_{r-1}\}$ and ω_s are the nonlinear weights corresponding to the substencils S_s with $s = 0, \dots, r-1$, which are used as the independent variables by the mapping function. Suppose that $(g^X)_s(\omega)$, $s = 0, \dots, r-1$ is the mapping function of the mapped WENO-X scheme, then we say that a **non-OP** mapping process occurs at x_j , if $\exists m, n \in \{0, \dots, r-1\}$, s.t.

$$\begin{cases} (\omega_m - \omega_n) \left((g^X)_m(\omega_m) - (g^X)_n(\omega_n) \right) < 0, & \text{if } \omega_m \neq \omega_n, \\ (g^X)_m(\omega_m) \neq (g^X)_n(\omega_n), & \text{if } \omega_m = \omega_n. \end{cases} \quad (23)$$

And we say x_j is a **non-OP point**. Otherwise, we say x_j is an **OP point**.

3.2. A general formula for the existing mapping functions

We rewrite the mapping function of the WENO-X scheme, that is, $(g^X)_s(\omega)$, $s = 0, 1, \dots, r-1$, to be a general formula, given as

$$g^X(\omega; m_p, P_{s,1}, \dots, P_{s,m_p}) = (g^X)_s(\omega), \quad (24)$$

where m_p is the number of the parameters related with s indicating the substencil, and $P_{s,1}, \dots, P_{s,m_p}$ are these parameters. Clearly, we have $m_p = 0$ for the WENO-JS scheme and $m_p \geq 1$ for other mapped WENO schemes. In Table 1, taking 9 different WENO schemes as examples, we have presented their parameters of m_p and $P_{s,1}, \dots, P_{s,m_p}$. Let n_X denote the order of the specified critical point, namely $\omega = d_s$, of the mapping function of the WENO-X scheme, that is, $(g^X)'_s(d_s) = \dots = (g^X)^{(n_X)}_s(d_s) = 0, (g^X)^{(n_X+1)}_s(d_s) \neq 0$. To simplify the description of Theorem 2 below, we present n_X of the WENO-X scheme in the sixth column of Table 1.

Lemma 2. For the WENO-X scheme shown in Table 1, the mapping function $(g^X)_s(\omega)$, $s = 0, 1, \dots, r-1$ is monotonically increasing over $[0, 1]$.

Proof. See the corresponding references given in the last column of Table 1. □

Table 1. The parameters m_p and $P_{s,1}, \dots, P_{s,m_p}$ for the WENO-JS scheme and some existing mapped WENO schemes whose mapping functions are *non-OP*.

No.	Scheme, WENO-X	m_p	$P_{s,1}, \dots, P_{s,m_p}$	Parameters	n_x	Ref.
1	WENO-JS	0	None	None	None	See [13]
2	WENO-M	1	$P_{s,1} = d_s$	None	2	See [11]
3	WENO-IM(k, A)	1	$P_{s,1} = d_s$	$k = 2.0, A = 0.1$	k	See [4]
4	WENO-PM k	1	$P_{s,1} = d_s$	$k = 6$	k	See [3]
5	WENO-PPM n	1	$P_{s,1} = d_s$	$n = 5$	4	See [15]
6	WENO-RM($mm0$)	1	$P_{s,1} = d_s$	$m = 2, n = 6$	3, 4	See [29]
7	WENO-MAIM1	2	$P_{s,1} = d_s, P_{s,2} = m_s$	$k = 10, A = 1.0e-6, m_s = 0.06$	$k, k + 1$	See [16]
8	WENO-ACM	2	$P_{s,1} = d_s, P_{s,2} = CFS_s$	$A = 20, k = 2, \mu = 1e-6, CFS_s = d_s/10$	∞	See [17]
9	MIP-WENO-ACM k	3	$P_{s,1} = d_s, P_{s,2} = CFS_s, P_{s,3} = k_s$	$k_s = 0.0, CFS_s = d_s/10$	∞	See [18]

3.3. The new mapping functions

Firstly, we give the **minDist** function by the following definition.

Definition 3. (*minDist function*) Define the **minDist** function as follows

$$\begin{cases} \mathbf{minDist}(x_0, \dots, x_{r-1}; d_0, \dots, d_{r-1}; \omega) = x_{k^*}, & (25a) \\ k^* = \min \left(\text{IndexOf} \left(\min \{ |\omega - d_0|, |\omega - d_1|, \dots, |\omega - d_{r-1}| \} \right) \right), & (25b) \end{cases}$$

where $d_s, s = 0, \dots, r-1$ is the optimal weight, ω is the nonlinear weight being the independent variable of the mapping function, and the function $\text{IndexOf}(\cdot)$ returns a set of the subscripts of “.”, that is, if $\min \{ |\omega - d_0|, |\omega - d_1|, \dots, |\omega - d_{r-1}| \} = |\omega - d_{m_1}| = |\omega - d_{m_2}| = \dots = |\omega - d_{m_M}|$, then

$$\text{IndexOf} \left(\min \{ |\omega - d_0|, |\omega - d_1|, \dots, |\omega - d_{r-1}| \} \right) = \{m_1, m_2, \dots, m_M\}. \quad (26)$$

Let $\mathcal{D} = \{d_0, d_1, \dots, d_{r-1}\}$ be an array of all the ideal weights of the $(2r-1)$ th-order WENO schemes. We build a new array by sorting the elements of \mathcal{D} in ascending order, that is, $\tilde{\mathcal{D}} = \{\tilde{d}_0, \tilde{d}_1, \dots, \tilde{d}_{r-1}\}$. In other words, the arrays \mathcal{D} and $\tilde{\mathcal{D}}$ have the same elements with different arrangements, and the elements of $\tilde{\mathcal{D}}$ satisfy

$$0 < \tilde{d}_0 < \tilde{d}_1 < \dots < \tilde{d}_{r-1} < 1. \quad (27)$$

Definition 4. Let $\mathcal{G} = \{(g^X)_0(\omega), (g^X)_1(\omega), \dots, (g^X)_{r-1}(\omega)\}$ be an array of all the mapping functions of the $(2r-1)$ th-order mapped WENO-X scheme. We define a new array by sorting the elements of \mathcal{G} in a new order, that is, $\tilde{\mathcal{G}} = \{(\tilde{g}^X)_0(\omega), (\tilde{g}^X)_1(\omega), \dots, (\tilde{g}^X)_{r-1}(\omega)\}$, where $(\tilde{g}^X)_s(\omega)$ is the mapping function associated with \tilde{d}_s .

Lemma 3. Denote $\tilde{d}_{-1} = 0, \tilde{d}_r = 1$. Let $\dot{d}_{-1} = \tilde{d}_{-1}, \dot{d}_0 = \frac{\tilde{d}_0 + \tilde{d}_1}{2}, \dots, \dot{d}_{r-2} = \frac{\tilde{d}_{r-2} + \tilde{d}_{r-1}}{2}, \dot{d}_{r-1} = \tilde{d}_r$. For $\forall i = 0, 1, \dots, r-1$, if $\omega \in (\dot{d}_{i-1}, \dot{d}_i]$, then

$$\min \left(\text{IndexOf} \left(\min \{ |\omega - \tilde{d}_0|, |\omega - \tilde{d}_1|, \dots, |\omega - \tilde{d}_{r-1}| \} \right) \right) = i.$$

Proof.

(1) We firstly prove the cases of $i = 1, \dots, r-2$. When $\tilde{d}_i \leq \omega \leq \frac{\tilde{d}_i + \tilde{d}_{i+1}}{2}$, as Eq.(27) holds, we get

$$\begin{cases} 0 \leq \omega - \tilde{d}_i \leq \tilde{d}_{i+1} - \omega < \dots < \tilde{d}_{r-1} - \omega, \\ 0 \leq \omega - \tilde{d}_i < \omega - \tilde{d}_{i-1} < \dots < \omega - \tilde{d}_0. \end{cases} \quad (28)$$

Similarly, when $\frac{\tilde{d}_{i-1} + \tilde{d}_i}{2} < \omega < \tilde{d}_i$, we get

$$\begin{cases} 0 < \tilde{d}_i - \omega < \omega - \tilde{d}_{i-1} < \cdots < \omega - \tilde{d}_0, \\ 0 < \tilde{d}_i - \omega < \tilde{d}_{i+1} - \omega < \cdots < \tilde{d}_{r-1} - \omega. \end{cases} \quad (29)$$

Then, according to Eq.(28)(29), we obtain

$$\min \{ |\omega - \tilde{d}_0|, \dots, |\omega - \tilde{d}_{i-1}|, |\omega - \tilde{d}_i|, |\omega - \tilde{d}_{i+1}|, \dots, |\omega - \tilde{d}_{r-1}| \} = |\omega - \tilde{d}_i| = |\omega - \tilde{d}_{i+1}|, \quad i = 1, \dots, r-2, \quad (30)$$

where the last equality holds if and only if $\omega - \tilde{d}_i = \tilde{d}_{i+1} - \omega$.

(2) For the case of $i = 0$, we know that $\omega \in (\tilde{d}_{-1}, \tilde{d}_0] = (0, \frac{\tilde{d}_0 + \tilde{d}_1}{2}]$. When $\tilde{d}_0 \leq \omega \leq \frac{\tilde{d}_0 + \tilde{d}_1}{2}$, we have

$$0 \leq \omega - \tilde{d}_0 \leq \tilde{d}_1 - \omega < \cdots < \tilde{d}_{r-1} - \omega. \quad (31)$$

And when $0 < \omega < \tilde{d}_0$, we have

$$0 < \tilde{d}_0 - \omega < \tilde{d}_1 - \omega < \cdots < \tilde{d}_{r-1} - \omega. \quad (32)$$

Then, according to Eq.(31)(32), we obtain

$$\min \{ |\omega - \tilde{d}_0|, \dots, |\omega - \tilde{d}_{i-1}|, |\omega - \tilde{d}_i|, |\omega - \tilde{d}_{i+1}|, \dots, |\omega - \tilde{d}_{r-1}| \} = |\omega - \tilde{d}_0| = |\omega - \tilde{d}_1|, \quad (33)$$

where the last equality holds if and only if $\omega - \tilde{d}_0 = \tilde{d}_1 - \omega$.

(3) As the proof of the case of $i = r-1$ is very similar to that of the case $i = 0$, we do not state it here for simplicity. And we can get that, if $\omega \in (\tilde{d}_{r-2}, \tilde{d}_{r-1}]$, then

$$\min \{ |\omega - \tilde{d}_0|, \dots, |\omega - \tilde{d}_{i-1}|, |\omega - \tilde{d}_i|, |\omega - \tilde{d}_{i+1}|, \dots, |\omega - \tilde{d}_{r-1}| \} = |\omega - \tilde{d}_{r-1}|. \quad (34)$$

(4) Thus, according to Eq.(3) and Eq.(30)(33)(34), we obtain

$$\min \left(\text{IndexOf} \left(\min \{ |\omega - \tilde{d}_0|, \dots, |\omega - \tilde{d}_{i-1}|, |\omega - \tilde{d}_i|, |\omega - \tilde{d}_{i+1}|, \dots, |\omega - \tilde{d}_{r-1}| \} \right) \right) = i.$$

Up to now, we have finished the proof of Lemma 3. \square

For simplicity of description and according to Lemma 3, we introduce intervals Ω_i defined as follows

$$\Omega_i = \{ \omega | \text{minDist}(\tilde{d}_0, \tilde{d}_1, \dots, \tilde{d}_{r-1}; \tilde{d}_0, \tilde{d}_1, \dots, \tilde{d}_{r-1}; \omega) = \tilde{d}_i \} = (\tilde{d}_{i-1}, \tilde{d}_i], \quad i = 0, 1, \dots, r-1. \quad (35)$$

If $\omega \in \Omega = (0, 1]$, it is trivial to verify that: (1) $\Omega = \Omega_0 \cup \Omega_1 \cup \cdots \cup \Omega_{r-1}$; (2) for $\forall i, j = 0, 1, \dots, r-1$ and $i \neq j$, $\Omega_i \cap \Omega_j = \emptyset$.

Lemma 4. Let $a, b \in \{0, 1, \dots, r-1\}$ and WENO-X the scheme shown in Table 1, for $\forall a \geq b$ and $\omega_\alpha \in \Omega_a, \omega_\beta \in \Omega_b$, we have the following properties: C1. if $a = b$ and $\omega_\alpha > \omega_\beta$, then $(\overline{g^X})_a(\omega_\alpha) \geq (\overline{g^X})_b(\omega_\beta)$; C2. if $a = b$ and $\omega_\alpha = \omega_\beta$, then $(\overline{g^X})_a(\omega_\alpha) = (\overline{g^X})_b(\omega_\beta)$; C3. if $a > b$, then $\omega_\alpha > \omega_\beta, (\overline{g^X})_a(\omega_\alpha) > (\overline{g^X})_b(\omega_\beta)$.

Proof. (1) We can directly get properties C1 and C2 from Lemma 2. (2) As $a > b$, according to Eq.(27)(35), we know that the interval Ω_a must be on the right side of the interval Ω_b , while $\omega_\alpha \in \Omega_a, \omega_\beta \in \Omega_b$ is given, then we get $\omega_\alpha > \omega_\beta$. Trivially, according to Definition 4, or by intuitively observing the curves of the mapping function $(\overline{g^X})_s(\omega)$ as shown in Fig. 1, we can obtain $(\overline{g^X})_a(\omega_\alpha) > (\overline{g^X})_b(\omega_\beta)$. Thus, C3 is proved. \square

By employing the **minDist** function, we build a general method to introduce the *OP* criterion into the existing mappings which are *non-OP*. The general method is stated in Algorithm 1.

Algorithm 1: A general method to construct *OP* mappings.

input : s , index indicating the substencil S_s and $s = 0, 1, \dots, r-1$
 d_s , optimal weights
 ω_s^{JS} , nonlinear weights computed by the WENO-JS scheme
 m_P , the number of the parameters related with s
 $P_{s,j}$, parameters related with s and $j = 1, \dots, m_P$

output: $\{(g^{\text{MOP-X}})_s(\omega_s^{\text{JS}}), s = 0, 1, \dots, r-1\}$, the new set of mapping functions that is *OP*

- 1 $(g^X)_s(\omega)$, $s = 0, 1, \dots, r-1$ is a monotonically increasing mapping function over $[0, 1]$, and the set of mapping functions $\{(g^X)_s(\omega), s = 0, 1, \dots, r-1\}$ is non-*OP*;
- 2 // implementation of the ‘‘minDist’’ function in Definition 3
- 3 **for** $s = 0; s \leq r-1; s++$ **do**
- 4 // get k^* in Eq. (25b)
- 5 set $d^{\min} = |\omega_s^{\text{JS}} - d_0|, k_s^* = 0$;
- 6 **for** $i = 1; i \leq r-1; i++$ **do**
- 7 **if** $|\omega_s^{\text{JS}} - d_i| < d^{\min}$ **then**
- 8 $d^{\min} = |\omega_s^{\text{JS}} - d_i|$,
- 9 $k_s^* = i$;
- 10 **end**
- 11 **end**
- 12 // remark: the for loop above indicates that $\omega_s^{\text{JS}} \in \Omega_{k_s^*}$
- 13 // get x_{k^*} in Eq. (25a)
- 14 **for** $j = 1; j \leq m_P; j++$ **do**
- 15 $\bar{P}_{s,j} = P_{k_s^*,j}$;
- 16 **end**
- 17 **end**
- 18 // get $(g^{\text{MOP-X}})_s(\omega_s^{\text{JS}})$
- 19 **for** $s = 0; s \leq r-1; s++$ **do**
- 20 $(g^{\text{MOP-X}})_s(\omega_s^{\text{JS}}) = g^X(\omega_s^{\text{JS}}; m_P, \bar{P}_{s,1}, \dots, \bar{P}_{s,m_P})$.
- 21 **end**

Theorem 1. The set of mapping functions $\{(g^{\text{MOP-X}})_s(\omega_s^{\text{JS}}), s = 0, 1, \dots, r-1\}$ obtained through Algorithm 1 is *OP*.

Proof. Let $\omega_m^{\text{JS}}, \omega_n^{\text{JS}} \in [0, 1]$ and $\forall m, n \in \{0, 1, \dots, r-1\}$. According to Algorithm 1 and without loss of generality, we can assume that $\omega_m^{\text{JS}} \in \Omega_{k_m^*}, \omega_n^{\text{JS}} \in \Omega_{k_n^*}$, and then we get

$$\begin{cases} (g^{\text{MOP-X}})_m(\omega_m^{\text{JS}}) = g^X(\omega_m^{\text{JS}}; m_P, P_{k_m^*,1}, \dots, P_{k_m^*,m_P}), \\ (g^{\text{MOP-X}})_n(\omega_n^{\text{JS}}) = g^X(\omega_n^{\text{JS}}; m_P, P_{k_n^*,1}, \dots, P_{k_n^*,m_P}). \end{cases}$$

It is easy to verify that

$$\begin{cases} g^X(\omega_m^{\text{JS}}; m_P, P_{k_m^*,1}, \dots, P_{k_m^*,m_P}) = (\widetilde{g^X})_{k_m^*}(\omega_m^{\text{JS}}), \\ g^X(\omega_n^{\text{JS}}; m_P, P_{k_n^*,1}, \dots, P_{k_n^*,m_P}) = (\widetilde{g^X})_{k_n^*}(\omega_n^{\text{JS}}). \end{cases}$$

Therefore, according to Lemma 4, we can finish the proof trivially. \square

We now define the modified weights which are *OP* as follows

$$\alpha_s^{\text{MOP-X}} = \frac{\alpha_s^{\text{MOP-X}}}{\sum_{l=0}^{r-1} \alpha_l^{\text{MOP-X}}}, \quad \alpha_s^{\text{MOP-X}} = (g^{\text{MOP-X}})_s(\omega_s^{\text{JS}}), \quad s = 0, \dots, r-1, \quad (36)$$

where $(g^{\text{MOP-X}})_s(\omega_s^{\text{JS}})$ is obtained from Algorithm 1. The associated scheme will be referred to as MOP-WENO-X.

The mapping functions of the WENO-X schemes presented in Table 1 and those of the corresponding MOP-WENO-X schemes are shown in Fig. 1. We can find that, for the mapping functions of the MOP-WENO-X schemes: (1) the monotonicity over the whole domain $(0, 1)$ is maintained; (2) the differentiability is reduced and limited to the neighborhood of the optimal weights d_s ; (3) the *OP* property is obtained. We summarize these properties as follows.

Theorem 2. Let $\bar{\Omega}_i = \{\omega \in \Omega_i \cap \omega \neq \partial\Omega_i\}$, $i = 0, 1, \dots, r-1$. The mapping function $(g^{\text{MOP-X}})_s(\omega)$ obtained from Algorithm 1 satisfies the following properties:

- C1. for $\forall \omega \in \bar{\Omega}_i, i = 0, 1, \dots, r-1$, $(g^{\text{MOP-X}})'_s(\omega) \geq 0$;
- C2. for $\forall \omega \in \Omega$, $0 \leq (g^{\text{MOP-X}})_s(\omega) \leq 1$;
- C3. for $\forall s \in \{0, 1, \dots, r-1\}$, $\tilde{d}_s \in \Omega_s$, and $(g^{\text{MOP-X}})_s(\tilde{d}_s) = \tilde{d}_s$, $(g^{\text{MOP-X}})'_s(\tilde{d}_s) = \dots = (g^{\text{MOP-X}})^{(n_x)}_s(\tilde{d}_s) = 0$ where n_x is given in Table 1;
- C4. $(g^{\text{MOP-X}})_s(0) = 0$, $(g^{\text{MOP-X}})_s(1) = 1$, $(g^{\text{MOP-X}})'_s(0) = (g^{\text{X}})'_s(0)$, $(g^{\text{MOP-X}})'_s(1) = (g^{\text{X}})'_s(1)$;
- C5. for $\forall m, n \in \{0, \dots, r-1\}$, if $\omega_m > \omega_n$, then $(g^{\text{MOP-X}})_m(\omega_m) \geq (g^{\text{MOP-X}})_n(\omega_n)$, and if $\omega_m = \omega_n$, then $(g^{\text{MOP-X}})_m(\omega_m) = (g^{\text{MOP-X}})_n(\omega_n)$.

3.4. Convergence properties

According to Theorem 2, we get the convergence properties for the $(2r-1)$ th-order MOP-WENO-X schemes as given in Theorem 3. The proof is almost identical with that of the corresponding WENO-X schemes in the references presented in Table 1.

Theorem 3. The requirements for the $(2r-1)$ th-order MOP-WENO-X schemes to achieve the optimal order of accuracy are identical with that of the corresponding $(2r-1)$ th-order WENO-X schemes.

For the integrity of this paper and for readers' convenience, we concisely express the following Corollaries of Theorem 3.

Corollary 1. If n mapping is used in the $(2r-1)$ th-order MOP-WENO-M scheme, then for different values of n_{cp} , the weights $\omega_s^{\text{MOP-M}}$ in the $(2r-1)$ th-order MOP-WENO-M scheme satisfy

$$\omega_s^{\text{MOP-M}} - d_s = O((\Delta x)^{3^n \times (r-1-n_{\text{cp}})}), \quad r = 2, 3, \dots, 9, \quad n_{\text{cp}} = 0, 1, \dots, r-1,$$

and the rate of convergence is

$$r_c = \begin{cases} 2r-1, & \text{if } n_{\text{cp}} = 0, \dots, \left\lfloor \frac{3^n-1}{3^n} r - 1 \right\rfloor, \\ (3^n+1)(r-1) - 3^n \times n_{\text{cp}}, & \text{if } n_{\text{cp}} = \left\lfloor \frac{3^n-1}{3^n} r - 1 \right\rfloor + 1, \dots, r-1. \end{cases}$$

where $\lfloor x \rfloor$ is a floor function of x .

Proof. The proof is almost identical with that of the Lemma 6 in [16]. □

Corollary 2. When $n_{\text{cp}} = 1$, the $(2r-1)$ th-order MOP-WENO-IM(k, A) schemes can achieve the optimal order of accuracy if the mapping function $(g^{\text{MOP-IM}})_s(\omega)$ is applied to the original weights in the $(2r-1)$ th-order WENO-JS schemes with requirement of $k \geq 2$ (except for the case $r = 2$).

Proof. The proof is almost identical with that of the Theorem 2 in [4]. □

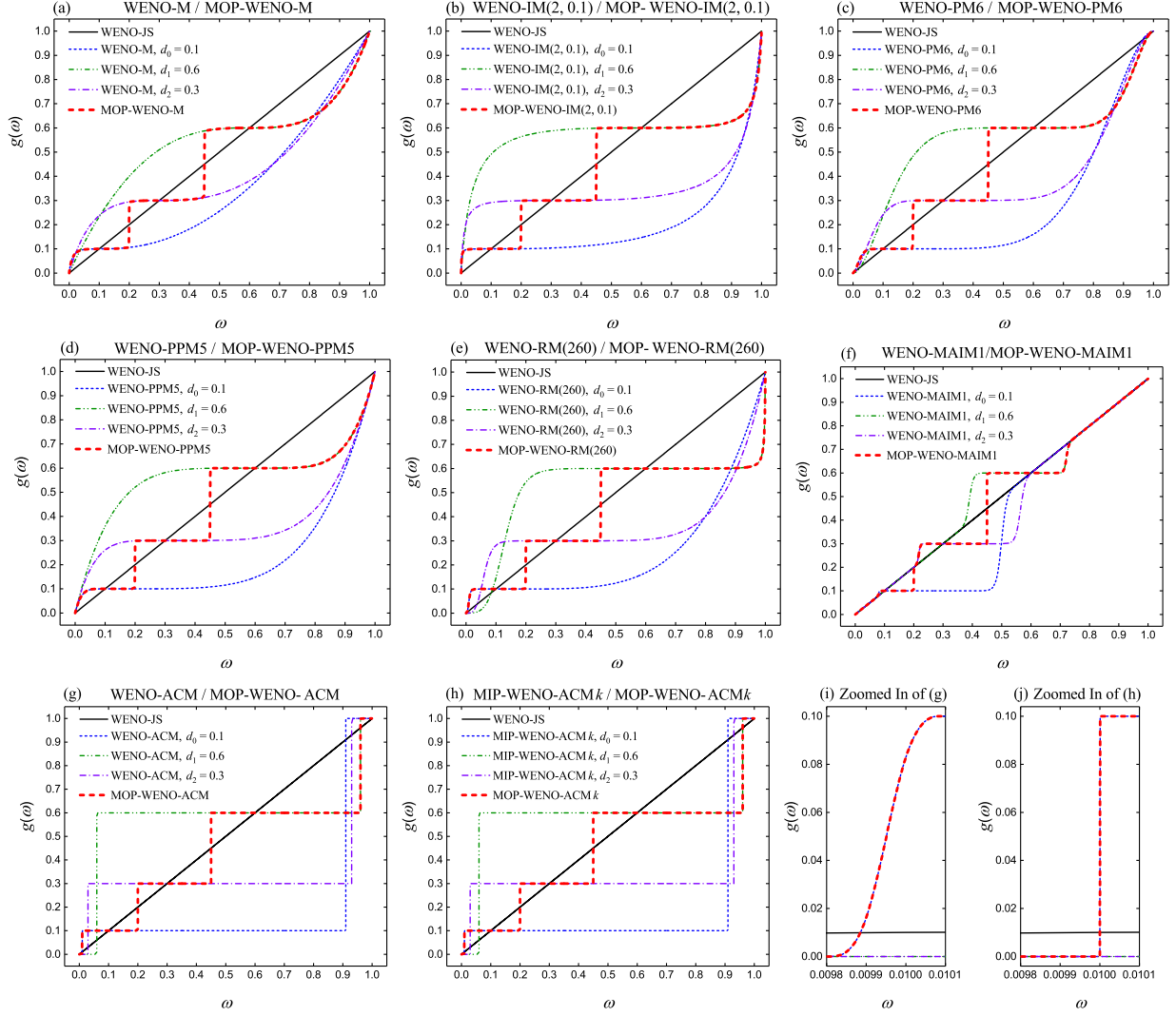


Fig. 1. Comparison for the mapping functions for WENO-X (shown in Table 1) and MOP-WENO-X.

Corollary 3. The $(2r - 1)$ th-order MOP-WENO-PM k schemes can achieve the optimal order of accuracy if the mapping function $(g^{\text{MOP-PM}})_s(\omega)$ is applied to the original weights in the $(2r - 1)$ th-order WENO-JS schemes with specific requirements for k in following different cases: (I) Require $k \geq 1$ for $n_{\text{cp}} = 0$; (II) Require $k \geq 1$ for $n_{\text{cp}} = 1$; (III) Require $k \geq 3$ for $n_{\text{cp}} = 2$.

Proof. The proof is almost identical with that of the Proposition 1 in [3]. □

Corollary 4. The $(2r - 1)$ th-order MOP-WENO-RM($mn0$) schemes can recover the optimal order of accuracy if the mapping function $(g^{\text{MOP-RM}})_s(\omega)$ is applied to the original weights in the $(2r - 1)$ th-order WENO-JS schemes with requirement of $n \geq \frac{1+n_{\text{cp}}}{r-1-n_{\text{cp}}}$ for different values of n_{cp} with $1 \leq n_{\text{cp}} < r - 1$.

Proof. The proof is almost identical with that of the Theorem 3 in [29]. □

Corollary 5. Let $\lceil x \rceil$ be a ceiling function of x , for $n_{cp} < r - 1$, the $(2r - 1)$ th-order MOP-WENO-MAIM1 schemes can achieve the optimal order of accuracy if the mapping function $(g^{\text{MOP-MAIM1}})_s(\omega)$ is applied to the original weights in the $(2r - 1)$ th-order WENO-JS schemes with requirement of $k \geq k^{\text{MAIM}}$, where

$$k^{\text{MAIM}} = \left\lceil \frac{r}{r-1-n_{cp}} - 2 \right\rceil + \frac{1 + (-1)^{\left\lceil \frac{r}{r-1-n_{cp}} - 2 \right\rceil}}{2}.$$

Proof. The proof is almost identical with that of the Theorem 2 in [16]. \square

Corollary 6. For $n_{cp} < r - 1$, the $(2r - 1)$ th-order MOP-WENO-ACM schemes can achieve the optimal order of accuracy if the mapping function $(g^{\text{MOP-ACM}})_s(\omega)$ is applied to the original weights in the $(2r - 1)$ th-order WENO-JS schemes.

Proof. The proof is almost identical with that of the Theorem 2 in [17]. \square

Corollary 7. When $\text{CFS}_s \ll \tilde{d}_0$, for $n_{cp} < r - 1$, the $(2r - 1)$ th-order MOP-WENO-ACMk schemes can achieve the optimal order of accuracy if the mapping function $(g^{\text{MOP-ACMk}})_s(\omega)$ is applied to the original weights in the $(2r - 1)$ th-order WENO-JS schemes.

Proof. The proof is almost identical with that of the Theorem 2 in [18]. \square

4. Numerical results

In this section, we compare the numerical performances of the MOP-WENO-X schemes with the corresponding existing mapped WENO-X schemes shown in Table 1, as well as the classic WENO-JS scheme. As the performances of the WENO-ACM scheme and the MOP-WENO-ACM scheme are almost identical to those of the MIP-WENO-ACMk scheme and the MOP-WENO-ACMk scheme respectively, we do not present the solutions of the WENO-ACM scheme and the MOP-WENO-ACM scheme below for simplicity. Typical one-dimensional linear advection equation and two-dimensional Euler equations, with different initial conditions, are used to test the considered schemes. The presentation of these numerical tests in this section starts with the accuracy test of one-dimensional linear advection equation with four different initial conditions, followed by the long output time simulations of it with two different initial conditions including discontinuities, and finishes with two-dimensional simulations on the shock-vortex interaction and the 2D Riemann problem. In all calculations below, ϵ is taken to be 10^{-40} for all schemes following the recommendations in [11, 4].

In the following numerical tests, the ODEs resulting from the semi-discretized PDEs are marched in time using the following explicit, third-order, strong stability preserving (SSP) Runge-Kutta method [26, 5, 6]

$$\begin{aligned}\vec{U}^* &= \vec{U}^n + \Delta t \mathcal{L}(\vec{U}^n), \\ \vec{U}^{**} &= \frac{3}{4}\vec{U}^n + \frac{1}{4}\vec{U}^* + \frac{1}{4}\Delta t \mathcal{L}(\vec{U}^*), \\ \vec{U}^{n+1} &= \frac{1}{3}\vec{U}^n + \frac{2}{3}\vec{U}^{**} + \frac{2}{3}\Delta t \mathcal{L}(\vec{U}^{**}),\end{aligned}$$

where \vec{U}^* , \vec{U}^{**} are the intermediate stages, \vec{U}^n is the value of \vec{U} at time level $t^n = n\Delta t$, and Δt is the time step satisfying some proper CFL condition. The spatial operator \mathcal{L} is defined as in Eq.(3), and the WENO reconstructions will be applied to obtain it.

4.1. Accuracy test

In this subsection, we solve the following one-dimensional linear advection equation

$$\frac{\partial u}{\partial t} + \frac{\partial u}{\partial x} = 0, \quad -1 \leq x \leq 1, \quad (37)$$

with different initial conditions to test the accuracy of the considered WENO schemes. In all accuracy tests, the L_1, L_2, L_∞ norms of the error are given as

$$\begin{aligned} L_1 &= h \cdot \sum_j |u_j^{\text{exact}} - (u_h)_j|, \\ L_2 &= \sqrt{h \cdot \sum_j (u_j^{\text{exact}} - (u_h)_j)^2}, \\ L_\infty &= \max_j |u_j^{\text{exact}} - (u_h)_j|, \end{aligned}$$

where $h = \Delta x$ is the uniform spatial step size, $(u_h)_j$ is the numerical solution and u_j^{exact} is the exact solution.

Example 1. We calculate Eq.(37) with the periodic boundary condition using the following initial condition [4]

$$u(x, 0) = \sin(\pi x). \quad (38)$$

It is trivial to verify that although the initial condition in Eq.(38) has two first-order critical points, their first and third derivatives vanish simultaneously. The CFL number is taken to be $(\Delta x)^{2/3}$ to prevent the convergence rates of error from being influenced by time advancement. The calculation is run until a time of $t = 2.0$.

In Table 2, we show the L_1, L_2, L_∞ errors and corresponding convergence orders of various considered WENO schemes. The results of the three rows are L_1 -, L_2 - and L_∞ - norm errors and convergence orders (in brackets) in turn (similarly hereinafter). Unsurprisingly, the MOP-WENO-X schemes and the corresponding WENO-X schemes provide more accurate results than the WENO-JS scheme do in general. Naturally and as expected, all the considered schemes have gained the fifth-order convergence rate of accuracy. It can be found that the results of the MOP-WENO-X schemes are identical to those of the corresponding WENO-X schemes for all grid numbers except $N = 10$. As discussed in [18], the cause of the accuracy loss for the computing cases of all MOP-WENO-X schemes with $N = 10$ is that the mapping functions of the MOP-WENO-X schemes have narrower optimal weight intervals (standing for the intervals about $\omega = d_s$ over which the mapping process attempts to use the corresponding optimal weights, see [16, 17]) than the corresponding WENO-X schemes.

Example 2. We calculate Eq.(37) with the periodic boundary condition using the following initial condition [11]

$$u(x, 0) = \sin\left(\pi x - \frac{\sin(\pi x)}{\pi}\right), \quad (39)$$

This particular initial condition has two first-order critical points, which both have a non-vanishing third derivative. Again, the CFL number is set to be $(\Delta x)^{2/3}$ and the calculation is run until a time of $t = 2.0$.

Table 3 compares the L_1, L_2, L_∞ errors and corresponding convergence orders obtained from the considered schemes. It is evident that the WENO-X schemes and the corresponding MOP-WENO-X schemes can achieve the optimal convergence orders. Unsurprisingly, the WENO-JS scheme gives less accurate results than the other schemes, and its L_∞ convergence order decreases by almost 2 orders leading to the noticeable drops of the L_1 and L_2 convergence orders. It is noteworthy that when the grid number is too small, like $N \leq 40$, in terms of accuracy, the MOP-WENO-X schemes provide less accurate results than those of the corresponding WENO-X schemes. As mentioned in Example 1, the cause of this kind of accuracy loss is that the mapping functions of the MOP-WENO-X schemes have narrower optimal weight intervals than the corresponding WENO-X schemes, and this issue can surely be addressed by increasing the grid number. Therefore, as expected, the MOP-WENO-X schemes show equally accurate numerical solutions as those of the corresponding WENO-X schemes when the grid number $N \geq 80$.

Example 3. We calculate Eq.(37) using the following initial condition [3]

Table 2. Convergence properties of considered schemes solving $u_t + u_x = 0$ with initial condition $u(x, 0) = \sin(\pi x)$.

N	10	20	40	80	160	320
WENO-JS	6.18628e-02(-)	2.96529e-03(4.3821)	9.27609e-05(4.9985)	2.89265e-06(5.0031)	9.03392e-08(5.0009)	2.82330e-09(4.9999)
	4.72306e-02(-)	2.42673e-03(4.2826)	7.64332e-05(4.9887)	2.33581e-06(5.0322)	7.19259e-08(5.0213)	2.23105e-09(5.0107)
	4.87580e-02(-)	2.57899e-03(4.2408)	9.05453e-05(4.8320)	2.90709e-06(4.9610)	8.85753e-08(5.0365)	2.72458e-09(5.0228)
WENO-M	2.01781e-02(-)	5.18291e-04(5.2829)	1.59422e-05(5.0228)	4.98914e-07(4.9979)	1.56021e-08(4.9990)	4.99356e-10(4.9977)
	1.55809e-02(-)	4.06148e-04(5.2616)	1.25236e-05(5.0193)	3.91875e-07(4.9981)	1.22541e-08(4.9991)	3.83568e-10(4.9976)
	1.47767e-02(-)	3.94913e-04(5.2256)	1.24993e-05(4.9816)	3.91808e-07(4.9956)	1.22538e-08(4.9988)	3.83541e-10(4.9977)
MOP-WENO-M	3.64427e-02(-)	5.18291e-04(6.1357)	1.59422e-05(5.0228)	4.98914e-07(4.9979)	1.56021e-08(4.9990)	4.88356e-10(4.9977)
	2.95270e-02(-)	4.06148e-04(6.1839)	1.25236e-05(5.0193)	3.91875e-07(4.9981)	1.22541e-08(4.9991)	3.83568e-10(4.9976)
	2.81876e-02(-)	3.94913e-04(6.1574)	1.24993e-05(4.9816)	3.91808e-07(4.9956)	1.22538e-08(4.9988)	3.83541e-10(4.9977)
WENO-IM(2,0,1)	1.58051e-02(-)	5.04401e-04(4.9697)	1.59160e-05(4.9860)	4.98863e-07(4.9957)	1.56020e-08(4.9988)	4.88355e-10(4.9977)
	1.23553e-02(-)	3.96236e-04(4.9626)	1.25033e-05(4.9860)	3.91836e-07(4.9959)	1.22541e-08(4.9989)	3.83568e-10(4.9976)
	1.19178e-02(-)	3.94458e-04(4.9171)	1.24963e-05(4.9803)	3.91797e-07(4.9953)	1.22538e-08(4.9988)	3.83547e-10(4.9977)
MOP-WENO-IM(2,0,1)	3.35513e-02(-)	5.04401e-04(6.0557)	1.59160e-05(4.9860)	4.98863e-07(4.9957)	1.56020e-08(4.9988)	4.88355e-10(4.9977)
	2.75968e-02(-)	3.96236e-04(6.1220)	1.25033e-05(4.9860)	3.91836e-07(4.9959)	1.22538e-08(4.9988)	3.83568e-10(4.9976)
	2.71898e-02(-)	3.94458e-04(6.1071)	1.24963e-05(4.9803)	3.91797e-07(4.9953)	1.22538e-08(4.9988)	3.83547e-10(4.9977)
WENO-PM6	1.74869e-02(-)	5.02923e-04(5.1198)	1.59130e-05(4.9821)	4.98858e-07(4.9954)	1.56020e-08(4.9988)	4.88355e-10(4.9977)
	1.35606e-02(-)	3.95215e-04(5.1006)	1.25010e-05(4.9825)	3.91831e-07(4.9957)	1.22541e-08(4.9989)	3.83568e-10(4.9976)
	1.27577e-02(-)	3.94515e-04(5.0151)	1.24960e-05(4.9805)	3.91795e-07(4.9952)	1.22538e-08(4.9988)	3.83543e-10(4.9977)
MOP-WENO-PM6	3.54584e-02(-)	5.02923e-04(6.1396)	1.59130e-05(4.9821)	4.98858e-07(4.9954)	1.56020e-08(4.9988)	4.88355e-10(4.9977)
	2.88246e-02(-)	3.95215e-04(6.1885)	1.25010e-05(4.9825)	3.91831e-07(4.9957)	1.22541e-08(4.9989)	3.83568e-10(4.9976)
	2.76902e-02(-)	3.94515e-04(6.1332)	1.24960e-05(4.9805)	3.91795e-07(4.9952)	1.22538e-08(4.9988)	3.83543e-10(4.9977)
WENO-PPM5	1.73978e-02(-)	5.03464e-04(5.1109)	1.59131e-05(4.9836)	4.98858e-07(4.9954)	1.56020e-08(4.9988)	4.88356e-10(4.9977)
	1.34998e-02(-)	3.95644e-04(5.0926)	1.25011e-05(4.9841)	3.91831e-07(4.9957)	1.22541e-08(4.9989)	3.83568e-10(4.9976)
	1.27018e-02(-)	3.94865e-04(5.0075)	1.24961e-05(4.9818)	3.91795e-07(4.9952)	1.22538e-08(4.9988)	3.83528e-10(4.9978)
MOP-WENO-PPM5	3.49872e-02(-)	5.03464e-04(6.1188)	1.59131e-05(4.9836)	4.98858e-07(4.9954)	1.56020e-08(4.9988)	4.88356e-10(4.9977)
	2.85173e-02(-)	3.95644e-04(6.1715)	1.25011e-05(4.9841)	3.91831e-07(4.9957)	1.22541e-08(4.9989)	3.83568e-10(4.9976)
	2.75955e-02(-)	3.94865e-04(6.1269)	1.24961e-05(4.9818)	3.91795e-07(4.9952)	1.22538e-08(4.9988)	3.83528e-10(4.9978)
WENO-RM(260)	1.52661e-02(-)	5.02845e-04(4.9241)	1.59130e-05(4.9818)	4.98858e-07(4.9954)	1.56020e-08(4.9988)	4.88355e-10(4.9977)
	1.19792e-02(-)	3.95138e-04(4.9220)	1.25010e-05(4.9822)	3.91831e-07(4.9957)	1.22541e-08(4.9989)	3.83568e-10(4.9976)
	1.17698e-02(-)	3.94406e-04(4.8993)	1.24960e-05(4.9801)	3.91795e-07(4.9952)	1.22538e-08(4.9988)	3.83543e-10(4.9977)
MOP-WENO-RM(260)	3.29243e-02(-)	5.02845e-04(6.0329)	1.59130e-05(4.9818)	4.98858e-07(4.9954)	1.56020e-08(4.9988)	4.88355e-10(4.9977)
	2.73131e-02(-)	3.95138e-04(6.1111)	1.25010e-05(4.9822)	3.91831e-07(4.9957)	1.22541e-08(4.9989)	3.83568e-10(4.9976)
	2.73015e-02(-)	3.94406e-04(6.1132)	1.24960e-05(4.9801)	3.91795e-07(4.9952)	1.22538e-08(4.9988)	3.83543e-10(4.9977)
WENO-MAIMI	6.13264e-02(-)	5.08205e-04(6.9150)	1.59130e-05(4.9971)	4.98858e-07(4.9954)	1.56020e-08(4.9988)	4.88355e-10(4.9977)
	4.81375e-02(-)	4.26155e-04(6.8196)	1.25010e-05(5.0913)	3.91831e-07(4.9957)	1.22541e-08(4.9989)	3.83568e-10(4.9976)
	4.86913e-02(-)	5.03701e-04(6.5950)	1.24960e-05(5.3330)	3.91795e-07(4.9952)	1.22538e-08(4.9988)	3.83543e-10(4.9977)
MOP-WENO-MAIMI	6.63923e-02(-)	5.08205e-04(7.0295)	1.59130e-05(4.9971)	4.98858e-07(4.9954)	1.56020e-08(4.9988)	4.88355e-10(4.9977)
	5.17462e-02(-)	4.26155e-04(6.9239)	1.25010e-05(5.0913)	3.91831e-07(4.9957)	1.22541e-08(4.9989)	3.83568e-10(4.9976)
	5.19799e-02(-)	5.03701e-04(6.6892)	1.24960e-05(5.3330)	3.91795e-07(4.9952)	1.22538e-08(4.9988)	3.83543e-10(4.9977)
MIP-WENO-ACMk	1.52184e-02(-)	5.02844e-04(4.9196)	1.59130e-05(4.9818)	4.98858e-07(4.9954)	1.56020e-08(4.9988)	4.88355e-10(4.9977)
	1.19442e-02(-)	3.95138e-04(4.9178)	1.25010e-05(4.9822)	3.91831e-07(4.9957)	1.22541e-08(4.9989)	3.83568e-10(4.9976)
	1.17569e-02(-)	3.94406e-04(4.8977)	1.24960e-05(4.9801)	3.91795e-07(4.9952)	1.22538e-08(4.9988)	3.83543e-10(4.9977)
MOP-WENO-ACMk	3.29609e-02(-)	5.02844e-04(6.0345)	1.59130e-05(4.9818)	4.98858e-07(4.9954)	1.56020e-08(4.9988)	4.88355e-10(4.9977)
	2.72363e-02(-)	3.95138e-04(6.1070)	1.25010e-05(4.9822)	3.91831e-07(4.9957)	1.22541e-08(4.9989)	3.83568e-10(4.9976)
	2.70295e-02(-)	3.94406e-04(6.0987)	1.24960e-05(4.9801)	3.91795e-07(4.9952)	1.22538e-08(4.9988)	3.83543e-10(4.9977)

$$u(x, 0) = \sin^9(\pi x), \quad (40)$$

with the periodic boundary condition. It is trivial to verify that this initial condition has high-order critical points. We also set the CFL number to be $(\Delta x)^{2/3}$.

Table 4 shows the L_1, L_2, L_∞ errors of the considered WENO schemes at several output times with a uniform mesh size of $\Delta x = 1/200$. In order to measure the dissipations of the schemes, as the authors did in [18], we give the corresponding increased errors (in percentage) compared to the MIP-WENO-ACMk scheme which gives solutions with very low dissipations. Taking the L_1 -norm error as an example, let $L_1^*(t)$ and $L_1^Y(t)$ the L_1 -norm errors of the MIP-WENO-ACMk scheme and the compared scheme, the increased errors at output time t is computed by $\frac{L_1^Y(t) - L_1^*(t)}{L_1^*(t)} \times 100\%$. From Table 4, we can observe that: (1) the WENO-JS scheme shows the largest increased errors for no matter short or long output times; (2) at short output times, like $t \leq 100$, the solutions computed by the WENO-M scheme are closer to those of the MIP-WENO-ACMk scheme, leading to smaller increased errors, than the corresponding MOP-WENO-M scheme; (3) however, when the output time is larger, like $t \geq 200$, the solutions computed by the MOP-WENO-M scheme, whose increased errors do not get larger but evidently decrease, are closer to those of the MIP-WENO-ACMk scheme than the corresponding WENO-M scheme whose errors increase dramatically leading to significantly larger increased errors; (4) although the errors of the MOP-WENO-X schemes except the MOP-WENO-M scheme are not as small as those of the corresponding WENO-X schemes, these errors can maintain a considerable level leading to acceptable increased errors that are much lower than those of the WENO-JS and WENO-M schemes.

Actually, as mentioned in Example 1 and Example 2, the cause of the slight accuracy loss discussed above is that the mapping function of the MOP-WENO-X schemes have narrower optimal weight intervals than the corresponding

Table 3. Convergence properties of considered schemes solving $u_t + u_x = 0$ with initial condition $u(x, 0) = \sin(\pi x) - \sin(\pi x)/\pi$.

N	10	20	40	80	160	320
WENO-JS	1.24488e-01(-)	1.01260e-02(3.6199)	7.22169e-04(3.8096)	3.42286e-05(4.3991)	1.58510e-06(4.4326)	7.95517e-08(4.3165)
	1.09463e-01(-)	8.72198e-03(3.6496)	6.76133e-04(3.6893)	3.63761e-05(4.2162)	2.29598e-06(3.9858)	1.68304e-07(3.7700)
WENO-M	1.24471e-01(-)	1.43499e-02(3.1167)	1.09663e-03(3.7099)	9.02485e-05(3.6030)	8.24022e-06(3.4531)	8.31702e-07(3.3085)
	7.53259e-02(-)	3.70838e-03(4.3443)	1.45082e-04(4.6758)	4.80253e-06(4.9169)	1.52120e-07(4.9805)	4.77083e-09(4.9948)
MOP-WENO-M	6.39017e-02(-)	3.36224e-03(4.2484)	1.39007e-04(4.5962)	4.52646e-06(4.9406)	1.42463e-07(4.9897)	4.45822e-09(4.9980)
	7.49250e-02(-)	5.43666e-03(3.7847)	2.18799e-04(4.6350)	6.81451e-06(5.0049)	2.14545e-07(4.9893)	6.71080e-09(4.9987)
WENO-IM(2.0.1)	9.41832e-02(-)	6.59540e-03(3.8359)	2.60456e-04(4.6623)	4.80253e-06(5.7611)	1.52120e-07(4.9805)	4.77083e-09(4.9948)
	8.03446e-02(-)	6.37937e-03(3.6547)	2.50868e-04(4.6684)	4.52646e-06(5.7924)	1.42463e-07(4.9897)	4.45822e-09(4.9980)
MOP-WENO-IM(2.0.1)	9.78919e-02(-)	8.97094e-03(3.4479)	4.10480e-04(4.4499)	6.81451e-06(5.9126)	2.14545e-07(4.9893)	6.71080e-09(4.9987)
	8.38131e-02(-)	4.30725e-03(4.2823)	1.51327e-04(4.8310)	4.85592e-06(4.9618)	1.52659e-07(4.9914)	4.77654e-09(4.9982)
WENO-PM6	6.71285e-02(-)	3.93700e-03(4.0918)	1.41737e-04(4.7958)	4.53602e-06(4.9656)	1.42479e-07(4.9926)	4.45805e-09(4.9986)
	7.62798e-02(-)	5.84039e-03(3.7072)	2.10531e-04(4.7940)	6.82606e-06(4.9468)	2.14534e-07(4.9918)	6.71079e-09(4.9986)
MOP-WENO-PM6	8.49795e-02(-)	7.01287e-03(3.5990)	2.59767e-04(4.7547)	4.85592e-06(5.7413)	1.52659e-07(4.9914)	4.77654e-09(4.9982)
	7.29388e-02(-)	6.80019e-03(3.4230)	2.51121e-04(4.5373)	4.53602e-06(5.7908)	1.42479e-07(4.9926)	4.45805e-09(4.9986)
WENO-PPM5	9.47429e-02(-)	9.96943e-03(3.2484)	4.01785e-04(4.6330)	6.82606e-06(5.8792)	2.14534e-07(4.9918)	6.71079e-09(4.9986)
	9.51313e-02(-)	4.82173e-03(4.3023)	1.55428e-04(4.9552)	4.87327e-06(4.9952)	1.52750e-07(4.9956)	4.77729e-09(4.9988)
MOP-WENO-PPM5	7.83600e-02(-)	4.29510e-03(4.1894)	1.43841e-04(4.9001)	4.54036e-06(4.9855)	1.42486e-07(4.9931)	4.45807e-09(4.9983)
	9.32356e-02(-)	5.91037e-03(3.9796)	2.09540e-04(4.8180)	6.83270e-06(4.9386)	2.14532e-07(4.9932)	6.71079e-09(4.9986)
WENO-PPM5	1.00298e-01(-)	5.84504e-03(4.1009)	2.51725e-04(4.5373)	4.87327e-06(5.6908)	1.52750e-07(4.9956)	4.77729e-09(4.9988)
	8.49034e-02(-)	5.80703e-03(3.8699)	2.40678e-04(4.5926)	4.54036e-06(5.7282)	1.42486e-07(4.9931)	4.45807e-09(4.9983)
MOP-WENO-PPM5	9.88357e-02(-)	9.01779e-03(3.4542)	3.66822e-04(4.6196)	6.83270e-06(5.7465)	2.14532e-07(4.9932)	6.71079e-09(4.9986)
	9.22982e-02(-)	4.68376e-03(4.3006)	1.55745e-04(4.9104)	4.88795e-06(4.9938)	1.52852e-07(4.9990)	4.77759e-09(4.9997)
WENO-RM(260)	7.46925e-02(-)	4.18882e-03(4.1563)	1.44018e-04(4.8622)	4.54528e-06(4.9857)	1.42506e-07(4.9953)	4.45812e-09(4.9984)
	8.46229e-02(-)	5.92748e-03(3.8356)	2.09420e-04(4.8229)	6.83617e-06(4.9371)	2.14527e-07(4.9940)	6.71080e-09(4.9985)
MOP-WENO-RM(260)	9.50369e-02(-)	6.27179e-03(3.9215)	2.52600e-04(4.6340)	4.88795e-06(5.6915)	1.52852e-07(4.9990)	4.77759e-09(4.9997)
	8.08190e-02(-)	6.11267e-03(3.7248)	2.41656e-04(4.6608)	4.54528e-06(5.7324)	1.42506e-07(4.9953)	4.45812e-09(4.9984)
WENO-MAIM1	9.65522e-02(-)	8.98120e-03(3.4263)	3.69338e-04(4.6039)	6.83617e-06(5.7556)	2.14527e-07(4.9940)	6.71080e-09(4.9985)
	8.24328e-02(-)	4.37642e-03(4.2354)	1.52200e-04(4.8457)	4.86434e-06(4.9676)	1.52735e-07(4.9931)	4.77728e-09(4.9987)
MOP-WENO-MAIM1	6.64590e-02(-)	4.00547e-03(4.0524)	1.42162e-04(4.8164)	4.53769e-06(4.9694)	1.42486e-07(4.9931)	4.45807e-09(4.9983)
	7.64206e-02(-)	5.88375e-03(3.6992)	2.09889e-04(4.8090)	6.83016e-06(4.9416)	2.14533e-07(4.9926)	6.71079e-09(4.9986)
WENO-ACMk	8.96509e-02(-)	6.87612e-03(3.7047)	2.59418e-04(4.7282)	4.86434e-06(5.7369)	1.52735e-07(4.9931)	4.77728e-09(4.9987)
	7.51169e-02(-)	6.65488e-03(3.4967)	2.51194e-04(4.7275)	4.53769e-06(5.7907)	1.42486e-07(4.9931)	4.45807e-09(4.9983)
MIP-WENO-ACMk	9.20962e-02(-)	9.75043e-03(3.2396)	4.03065e-04(4.5964)	6.83016e-06(5.8829)	2.14533e-07(4.9926)	6.71079e-09(4.9986)
	1.24659e-01(-)	8.07923e-03(3.9476)	3.32483e-04(4.6029)	1.01162e-05(5.0385)	1.52910e-07(6.0478)	4.77728e-09(5.0003)
MOP-WENO-ACMk	1.14152e-01(-)	7.08117e-03(4.0108)	3.36264e-04(4.3963)	1.49724e-05(4.4892)	1.42515e-07(6.7150)	4.45807e-09(4.9986)
	1.40438e-01(-)	1.03772e-02(3.7584)	6.62891e-04(3.9685)	4.48554e-05(3.8854)	2.14522e-07(7.7080)	6.71079e-09(4.9985)
WENO-ACMk	1.27999e-01(-)	7.62753e-03(4.0688)	3.37132e-04(4.4998)	1.01162e-05(5.0586)	1.52910e-07(6.0478)	4.77728e-09(5.0003)
	1.12692e-01(-)	6.93240e-03(4.0229)	3.36497e-04(4.3647)	1.49724e-05(4.4902)	1.42515e-07(6.7150)	4.45807e-09(4.9986)
MOP-WENO-ACMk	1.31113e-01(-)	1.27480e-02(3.3625)	6.40953e-04(4.3139)	4.48554e-05(3.8369)	2.14522e-07(7.7080)	6.71079e-09(4.9985)
	8.75629e-02(-)	4.39527e-03(4.3163)	1.52219e-04(4.8517)	4.86436e-06(4.9678)	1.52735e-07(4.9931)	4.77728e-09(4.9987)
WENO-ACMk	6.98131e-02(-)	4.02909e-03(4.1150)	1.42172e-04(4.8247)	4.53770e-06(4.9695)	1.42486e-07(4.9931)	4.45807e-09(4.9983)
	7.91292e-02(-)	5.89045e-03(3.7478)	2.09893e-04(4.8107)	6.83017e-06(4.9416)	2.14533e-07(4.9926)	6.71079e-09(4.9986)
MOP-WENO-ACMk	9.08634e-02(-)	7.09246e-03(3.6793)	2.59429e-04(4.7729)	4.86436e-06(5.7369)	1.52735e-07(4.9931)	4.77728e-09(4.9987)
	7.58160e-02(-)	6.88532e-03(3.4609)	2.51208e-04(4.7766)	4.53770e-06(5.7908)	1.42486e-07(4.9931)	4.45807e-09(4.9983)
	9.29135e-02(-)	1.01479e-02(3.1947)	4.03069e-04(4.6540)	6.83017e-06(5.8830)	2.14533e-07(4.9926)	6.71079e-09(4.9986)

WENO-X schemes, and one can easily overcome this drawback by increasing the grid number. To demonstrate this, we calculate this problem using the same schemes at the same output times with a larger grid number of $N = 800$. The results are shown in Table 5, and we can see that: (1) the errors of the MOP-WENO-X schemes get closer to those of the MIP-WENO-ACMk scheme when the grid number increases from $N = 200$ to $N = 800$, resulting in the significantly decrease of the increased errors, and in different words, the errors of the MOP-WENO-X schemes and the MIP-WENO-ACMk scheme are so close that one can ignore their differences; (2) although the errors of the WENO-JS and WENO-M schemes get smaller when the grid number increases from $N = 200$ to $N = 800$, their increased errors become very very large; (3) naturally, the increased errors of the MOP-WENO-X schemes are extremely smaller than those of the WENO-JS and WENO-M schemes. Actually, it is an important advantage of the MOP-WENO-X schemes that can maintain comparably high resolution for long output times. In next subsection we will make a further discussion for this.

In Fig. 2 and Fig. 3, we plot the solutions computed by various schemes at output time $t = 1000$ with the grid number of $N = 200$ and $N = 800$, respectively. For $N = 200$, Fig. 2 shows that: (1) the MOP-WENO-M scheme provides result with far higher resolution than the corresponding WENO-M scheme which gives result with slightly better resolution than the lowest one computed by the WENO-JS scheme; (2) the result of the MOP-WENO-MAIM1 scheme are very close to that of its corresponding WENO-MAIM1 scheme; (3) look at the results of the other MOP-WENO-X schemes, they show far better resolutions than the WENO-M and WENO-JS schemes, although they give results with very slightly lower resolutions than their corresponding WENO-X schemes because of the narrower optimal weight intervals. Actually, we can amend this minor issue by using a larger grid number. Consequently, for

$N = 800$, it can be seen from Fig. 3 that all the MOP-WENO-X schemes produce results very close to those of their corresponding mapped WENO-X schemes with extremely high resolutions except the WENO-M and WENO-JS schemes, whose resolutions are much lower.

Table 4. Performance of various considered schemes solving $u_t + u_x = 0$ with $u(x, 0) = \sin^9(\pi x)$, $\Delta x = 1/200$.

Scheme	$t = 10$	$t = 100$	$t = 200$	$t = 500$	$t = 1000$
WENO-JS	3.86931e-04(359.06%)	5.42288e-03(548.87%)	2.35657e-02(1323.42%)	1.55650e-01(3832.05%)	2.91359e-01(3920.28%)
	3.52611e-04(330.48%)	5.17716e-03(539.41%)	2.68753e-02(1580.45%)	1.46859e-01(3716.48%)	2.66692e-01(3595.71%)
WENO-M	5.36940e-04(288.51%)	1.20056e-02(780.15%)	6.47820e-02(2308.66%)	2.57663e-01(3891.29%)	4.44664e-01(3556.96%)
	8.90890e-05(5.70%)	1.29154e-03(54.54%)	5.74021e-03(246.72%)	4.89290e-02(1136.05%)	1.34933e-01(1761.86%)
MOP-WENO-M	8.32089e-05(1.58%)	1.28740e-03(59.00%)	7.66721e-03(379.41%)	6.23842e-02(1521.20%)	1.46524e-01(1930.47%)
	1.38348e-04(0.10%)	3.32665e-03(143.88%)	2.37125e-02(781.65%)	1.78294e-01(2661.83%)	3.17199e-01(2508.69%)
WENO-IM(2, 0.1)	1.56466e-04(85.63%)	2.88442e-03(245.13%)	5.11795e-03(209.14%)	9.09352e-03(129.72%)	1.75990e-02(142.84%)
	1.63200e-04(99.24%)	3.40815e-03(320.93%)	4.87507e-03(204.83%)	8.61108e-03(123.78%)	1.70893e-02(136.82%)
MOP-WENO-IM(2, 0.1)	5.08956e-04(268.26%)	1.01393e-02(643.33%)	1.02172e-02(279.89%)	1.98022e-02(108.74%)	4.01776e-02(230.43%)
	8.46989e-05(0.49%)	8.39425e-04(0.44%)	1.67834e-03(1.38%)	4.17514e-03(5.47%)	8.13666e-03(12.27%)
WENO-PM6	8.20061e-05(0.12%)	8.10915e-04(0.15%)	1.60667e-03(0.46%)	3.93647e-03(2.30%)	7.71028e-03(6.85%)
	1.38220e-04(0.01%)	1.36420e-03(0.01%)	2.68977e-03(0.01%)	6.45231e-03(-0.05%)	1.21388e-02(-0.17%)
MOP-WENO-PM6	1.55777e-04(84.82%)	2.74109e-03(227.98%)	4.16210e-03(151.40%)	8.37898e-03(111.67%)	1.25166e-02(72.71%)
	1.62626e-04(98.54%)	3.25705e-03(302.26%)	3.76225e-03(135.25%)	8.02344e-03(108.51%)	1.14682e-02(58.92%)
WENO-PPM5	5.08361e-04(267.83%)	9.88287e-03(624.53%)	6.81406e-03(153.35%)	1.84998e-02(186.57%)	2.02754e-02(66.75%)
	8.40259e-05(-0.31%)	8.30374e-04(-0.64%)	1.63963e-03(-0.96%)	3.88864e-03(-1.76%)	7.17606e-03(-0.98%)
MOP-WENO-PPM5	8.19676e-05(0.07%)	8.09152e-04(-0.07%)	1.59697e-03(-0.15%)	3.83159e-03(-0.43%)	1.79008e-03(-0.36%)
	1.38205e-04(0.00%)	1.36410e-03(0.00%)	2.68938e-03(-0.01%)	6.45650e-03(0.01%)	1.21637e-02(0.04%)
WENO-PPM5	1.53937e-04(82.63%)	2.70283e-03(223.40%)	4.07454e-03(146.11%)	8.46326e-03(113.80%)	1.54196e-02(112.77%)
	1.59169e-04(94.32%)	3.19156e-03(294.18%)	3.66635e-03(129.25%)	8.02943e-03(108.66%)	1.49590e-02(107.30%)
MOP-WENO-PPM5	4.92116e-04(256.08%)	9.52154e-03(598.04%)	6.49923e-03(141.65%)	1.83171e-02(183.74%)	3.15065e-02(159.11%)
	8.40198e-05(-0.32%)	8.30119e-04(-0.67%)	1.63931e-03(-0.98%)	3.89396e-03(-1.63%)	7.20573e-03(-0.57%)
WENO-RM(260)	8.19609e-05(0.06%)	8.09118e-04(-0.07%)	1.59692e-03(-0.15%)	3.83250e-03(-0.40%)	7.19622e-03(-0.28%)
	1.38206e-04(0.00%)	1.36411e-03(0.01%)	2.68939e-03(-0.01%)	6.45658e-03(0.01%)	1.21629e-02(0.03%)
MOP-WENO-RM(260)	1.53322e-04(81.90%)	2.70476e-03(223.63%)	4.17894e-03(152.42%)	8.34997e-03(110.94%)	1.21149e-02(67.17%)
	1.59164e-04(94.31%)	3.20725e-03(296.11%)	3.78313e-03(136.55%)	7.98345e-03(107.47%)	1.09845e-02(52.22%)
WENO-MAIM1	4.97691e-04(260.11%)	9.71919e-03(612.53%)	6.89990e-03(156.54%)	1.83470e-02(184.20%)	1.87607e-02(54.29%)
	8.43348e-05(0.06%)	8.35534e-04(-0.03%)	1.65314e-03(-0.15%)	3.94006e-03(-0.47%)	7.25689e-03(0.13%)
MOP-WENO-MAIM1	8.19287e-05(0.02%)	8.09704e-04(0.00%)	1.59924e-03(0.00%)	3.84494e-03(-0.08%)	7.22386e-03(0.11%)
	1.38206e-04(0.00%)	1.36404e-03(0.00%)	2.68956e-03(0.00%)	6.45544e-03(0.00%)	1.21576e-02(-0.01%)
WENO-ACMk	1.55787e-04(84.83%)	2.72147e-03(225.63%)	4.13179e-03(149.57%)	8.32505e-03(110.31%)	1.57577e-02(117.43%)
	1.62604e-04(98.51%)	3.22596e-03(298.42%)	3.73345e-03(133.44%)	7.96768e-03(107.06%)	1.53795e-02(113.12%)
MOP-WENO-ACMk	5.05390e-04(265.68%)	9.74612e-03(614.50%)	6.71615e-03(149.71%)	1.83262e-02(183.88%)	3.30552e-02(171.85%)
	8.24623e-05(-2.17%)	8.03920e-04(-3.81%)	1.58626e-03(-4.19%)	3.77900e-03(-4.53%)	7.04287e-03(-2.82%)
WENO-ACMk	8.18028e-05(-0.13%)	8.04763e-04(-0.61%)	1.58610e-03(-0.82%)	3.79788e-03(-1.30%)	7.14409e-03(-1.00%)
	1.38215e-04(0.01%)	1.36392e-03(-0.01%)	2.68849e-03(-0.04%)	6.46356e-03(0.12%)	1.21473e-02(-0.10%)
MOP-WENO-ACMk	9.97376e-05(18.33%)	8.16839e-04(-2.26%)	1.60912e-03(-2.81%)	6.83393e-03(72.64%)	1.24817e-02(72.23%)
	8.85740e-05(8.13%)	8.07516e-04(-0.27%)	1.59351e-03(-0.36%)	6.96428e-03(80.98%)	1.20092e-02(66.42%)
MIP-WENO-ACMk	1.38172e-04(-0.02%)	1.36470e-03(0.05%)	2.68832e-03(-0.05%)	1.63188e-02(152.78%)	2.22178e-02(82.72%)
	8.42873e-05(-)	8.35747e-04(-)	1.65557e-03(-)	3.95849e-03(-)	7.24723e-03(-)
MOP-WENO-ACMk	8.19107e-05(-)	8.09679e-04(-)	1.59929e-03(-)	3.84802e-03(-)	7.21626e-03(-)
	1.38205e-04(-)	1.36404e-03(-)	2.68955e-03(-)	6.45564e-03(-)	1.21593e-02(-)
MOP-WENO-ACMk	1.55900e-04(84.96%)	2.72470e-03(226.02%)	4.11740e-03(148.70%)	8.34435e-03(110.80%)	1.54830e-02(113.64%)
	1.63558e-04(99.68%)	3.23726e-03(299.82%)	3.71649e-03(132.38%)	7.96980e-03(107.11%)	1.50017e-02(107.89%)
	5.22964e-04(278.40%)	9.83147e-03(620.76%)	6.66166e-03(147.69%)	1.83215e-02(183.81%)	3.16523e-02(160.31%)

Example 4. We calculate Eq.(37) using the following initial condition [13]

$$u(x, 0) = \begin{cases} \frac{1}{6}[G(x, \beta, z - \hat{\delta}) + 4G(x, \beta, z) + G(x, \beta, z + \hat{\delta})], & x \in [-0.8, -0.6], \\ 1, & x \in [-0.4, -0.2], \\ 1 - |10(x - 0.1)|, & x \in [0.0, 0.2], \\ \frac{1}{6}[F(x, \alpha, a - \hat{\delta}) + 4F(x, \alpha, a) + F(x, \alpha, a + \hat{\delta})], & x \in [0.4, 0.6], \\ 0, & \text{otherwise,} \end{cases} \quad (41)$$

where $G(x, \beta, z) = e^{-\beta(x-z)^2}$, $F(x, \alpha, a) = \sqrt{\max(1 - \alpha^2(x-a)^2, 0)}$, and the constants are $z = -0.7$, $\hat{\delta} = 0.005$, $\beta = \frac{\log 2}{36\hat{\delta}^2}$, $a = 0.5$ and $\alpha = 10$. The periodic boundary condition is used and the CFL number is taken to be 0.1. For brevity in the presentation, we call this *Linear Problem SLP* as it is presented by *Shu* et al. in [13]. It is known that this problem consists of a Gaussian, a square wave, a sharp triangle and a semi-ellipse.

In Table 6, we present the L_1 , L_2 , L_∞ errors and the corresponding convergence rates of accuracy with $t = 2, 2000$. For the case of $t = 2$, it can be seen that: (1) the L_1 and L_2 orders of all considered schemes are approximately 1.0

Table 5. Performance of various considered schemes solving $u_t + u_x = 0$ with $u(x, 0) = \sin^9(\pi x)$, $\Delta x = 1/800$.

Scheme	$t = 10$	$t = 100$	$t = 200$	$t = 500$	$t = 1000$
WENO-JS	4.23531e-07(411.02%)	4.74028e-06(471.88%)	7.29285e-05(4299.06%)	3.11698e-02(751974.43%)	1.01278e-01(1221783.34%)
	3.76804e-07(367.05%)	4.32403e-06(435.83%)	1.60499e-04(9844.24%)	4.08456e-02(1012202.60%)	1.13316e-01(1404171.46%)
	6.95290e-07(410.60%)	1.09481e-05(703.79%)	9.51604e-04(34832.14%)	8.63989e-02(1268572.78%)	2.13485e-01(1567406.64%)
WENO-M	8.28912e-08(0.01%)	8.29015e-07(0.01%)	2.27991e-06(37.52%)	1.41413e-03(34020.56%)	1.83325e-02(221075.14%)
	8.06774e-08(0.00%)	8.06977e-07(0.00%)	2.59031e-06(60.49%)	3.28891e-03(81411.16%)	3.30753e-02(409786.51%)
	1.36173e-07(0.00%)	1.36207e-06(0.00%)	1.22731e-05(350.53%)	1.90785e-02(280046.78%)	1.38215e-01(1014739.13%)
MOP-WENO-M	8.48762e-08(2.41%)	9.93577e-07(19.87%)	1.81123e-06(9.25%)	4.68314e-06(13.00%)	8.53126e-06(2.93%)
	8.11503e-08(0.59%)	9.29166e-07(15.14%)	1.65928e-06(2.81%)	4.27588e-06(5.97%)	8.12198e-06(0.65%)
	1.36173e-07(0.00%)	2.03738e-06(49.58%)	2.72417e-06(0.00%)	6.81022e-06(0.00%)	1.36195e-05(0.00%)
WENO-IM(2, 0.1)	8.28803e-08(0.00%)	8.28891e-07(0.00%)	1.65781e-06(0.00%)	4.14443e-06(0.00%)	8.28840e-06(0.00%)
	8.06769e-08(0.00%)	8.06974e-07(0.00%)	1.61399e-06(0.00%)	4.03492e-06(0.00%)	8.06939e-06(0.00%)
	1.36172e-07(0.00%)	1.36206e-06(0.00%)	2.72415e-06(0.00%)	6.81019e-06(0.00%)	1.36194e-05(0.00%)
MOP-WENO-IM(2, 0.1)	8.48292e-08(2.35%)	9.80868e-07(18.33%)	1.79137e-06(8.06%)	4.88306e-06(17.82%)	8.63424e-06(4.17%)
	8.11341e-08(0.57%)	9.16723e-07(13.60%)	1.65133e-06(2.31%)	4.51320e-06(11.85%)	8.15362e-06(1.04%)
	1.36172e-07(0.00%)	1.87953e-06(37.99%)	2.72415e-06(0.00%)	9.14624e-06(34.30%)	1.36194e-05(0.00%)
WENO-PM6	8.28795e-08(0.00%)	8.28892e-07(0.00%)	1.65782e-06(0.00%)	4.14452e-06(0.00%)	8.84565e-06(6.72%)
	8.06769e-08(0.00%)	8.06973e-07(0.00%)	1.61399e-06(0.00%)	4.03492e-06(0.00%)	8.31248e-06(3.01%)
	1.36172e-07(0.00%)	1.36206e-06(0.00%)	2.72415e-06(0.00%)	6.81018e-06(0.00%)	1.38461e-05(1.66%)
MOP-WENO-PM6	8.47719e-08(2.28%)	9.71688e-07(17.23%)	1.78163e-06(7.47%)	4.93547e-06(19.08%)	8.65269e-06(4.39%)
	8.11105e-08(0.54%)	9.05382e-07(12.19%)	1.64687e-06(2.04%)	4.61707e-06(14.43%)	8.15964e-06(1.12%)
	1.36172e-07(0.00%)	1.78452e-06(31.02%)	2.72415e-06(0.00%)	1.08735e-05(59.67%)	1.36194e-05(0.00%)
WENO-PPM5	8.28794e-08(0.00%)	8.28890e-07(0.00%)	1.65781e-06(0.00%)	4.14448e-06(0.00%)	8.28862e-06(0.00%)
	8.06769e-08(0.00%)	8.06973e-07(0.00%)	1.61399e-06(0.00%)	4.03492e-06(0.00%)	8.06938e-06(0.00%)
	1.36172e-07(0.00%)	1.36206e-06(0.00%)	2.72415e-06(0.00%)	6.81018e-06(0.00%)	1.36194e-05(0.00%)
MOP-WENO-PPM5	8.47367e-08(2.24%)	1.04103e-06(25.59%)	1.83725e-06(10.82%)	4.30721e-06(3.93%)	8.27506e-06(-0.16%)
	8.10958e-08(0.52%)	1.00371e-06(24.38%)	1.67934e-06(4.05%)	4.06082e-06(0.64%)	8.07071e-06(0.02%)
	1.36172e-07(0.00%)	1.78285e-06(30.89%)	2.72415e-06(0.00%)	6.81018e-06(0.00%)	1.36194e-05(0.00%)
WENO-RM(260)	8.28794e-08(0.00%)	8.28889e-07(0.00%)	1.65781e-06(0.00%)	4.14448e-06(0.00%)	8.28860e-06(0.00%)
	8.06769e-08(0.00%)	8.06973e-07(0.00%)	1.61399e-06(0.00%)	4.03492e-06(0.00%)	8.06938e-06(0.00%)
	1.36172e-07(0.00%)	1.36206e-06(0.00%)	2.72415e-06(0.00%)	6.81018e-06(0.00%)	1.36194e-05(0.00%)
MOP-WENO-RM(260)	8.48225e-08(2.34%)	9.56819e-07(15.43%)	1.77008e-06(6.77%)	4.72311e-06(13.96%)	8.55573e-06(3.22%)
	8.11306e-08(0.56%)	8.87179e-07(9.94%)	1.64102e-06(1.67%)	4.33993e-06(7.56%)	8.12608e-06(0.70%)
	1.36172e-07(0.00%)	1.58577e-06(16.42%)	2.72415e-06(0.00%)	6.81018e-06(0.00%)	1.36194e-05(0.00%)
WENO-MAIM1	8.28796e-08(0.00%)	8.28893e-07(0.00%)	1.65782e-06(0.00%)	4.14450e-06(0.00%)	8.28865e-06(0.00%)
	8.06776e-08(0.00%)	8.06974e-07(0.00%)	1.61399e-06(0.00%)	4.03492e-06(0.00%)	8.06938e-06(0.00%)
	1.36172e-07(0.00%)	1.36206e-06(0.00%)	2.72415e-06(0.00%)	6.81018e-06(0.00%)	1.36194e-05(0.00%)
MOP-WENO-MAIM1	8.28791e-08(0.00%)	8.28894e-07(0.00%)	1.65783e-06(0.00%)	4.14454e-06(0.00%)	8.28830e-06(0.00%)
	8.06770e-08(0.00%)	8.06973e-07(0.00%)	1.61399e-06(0.00%)	4.03491e-06(0.00%)	8.06937e-06(0.00%)
	1.36172e-07(0.00%)	1.36206e-06(0.00%)	2.72415e-06(0.00%)	6.81018e-06(0.00%)	1.36194e-05(0.00%)
MIP-WENO-ACMk	8.28794e-08(-)	8.28891e-07(-)	1.65782e-06(-)	4.14451e-06(-)	8.28868e-06(-)
	8.06769e-08(-)	8.06973e-07(-)	1.61399e-06(-)	4.03492e-06(-)	8.06938e-06(-)
	1.36172e-07(-)	1.36206e-06(-)	2.72415e-06(-)	6.81018e-06(-)	1.36194e-05(-)
MOP-WENO-ACMk	8.47930e-08(2.31%)	9.73202e-07(17.41%)	1.78369e-06(7.59%)	4.84739e-06(16.96%)	8.61232e-06(3.90%)
	8.11193e-08(0.55%)	9.07161e-07(12.42%)	1.64768e-06(2.09%)	4.47345e-06(10.87%)	8.14436e-06(0.93%)
	1.36172e-07(0.00%)	1.79160e-06(31.54%)	2.72415e-06(0.00%)	8.79296e-06(29.11%)	1.36194e-05(0.00%)

and about 0.35 to 0.5, respectively; (2) negative values of the L_∞ orders of all considered schemes are generated; (3) in terms of accuracy, the MOP-WENO-X schemes produce less accurate results than the corresponding WENO-X schemes. For the case of $t = 2000$, it can be seen that: (1) the L_1 , L_2 orders of the WENO-JS and WENO-M schemes decrease to very small values and even become negative; (2) however, the L_1 and L_2 orders of all the MOP-WENO-X schemes, as well as the corresponding mapped WENO-X schemes except WENO-M, are clearly larger than 1.0 and around 0.5 to 0.9 respectively; (3) the L_∞ orders of all WENO-X schemes are very small and some of them even become negative (e.g., the WENO-JS, WENO-PPM5 and MIP-WENO-ACMk schemes), while those of the MOP-WENO-X schemes are all positive although they are also very small; (4) in terms of accuracy, on the whole, the MOP-WENO-X schemes produce accurate and comparable results as the corresponding WENO-X schemes except the WENO-M scheme. However, if we take a closer look, we can find that the resolution of the result computed by the WENO-M scheme is significantly lower than that of the MOP-WENO-M scheme, and the other mapped WENO-X schemes generate spurious oscillations but the corresponding MOP-WENO-X schemes do not. Detailed tests will be conducted and the solutions will be presented carefully to demonstrate this in the following subsection.

4.2. 1D linear advection problems with long output times

The objective of this subsection is to demonstrate the advantage of the MOP-WENO-X schemes on long output time simulations that can obtain high resolution and meanwhile do not generate spurious oscillations.

The one-dimensional linear advection problem Eq.(37) is solved with the periodic boundary condition by taking the following two initial conditions.

Case 1. (SLP) The initial condition is given by Eq.(41).

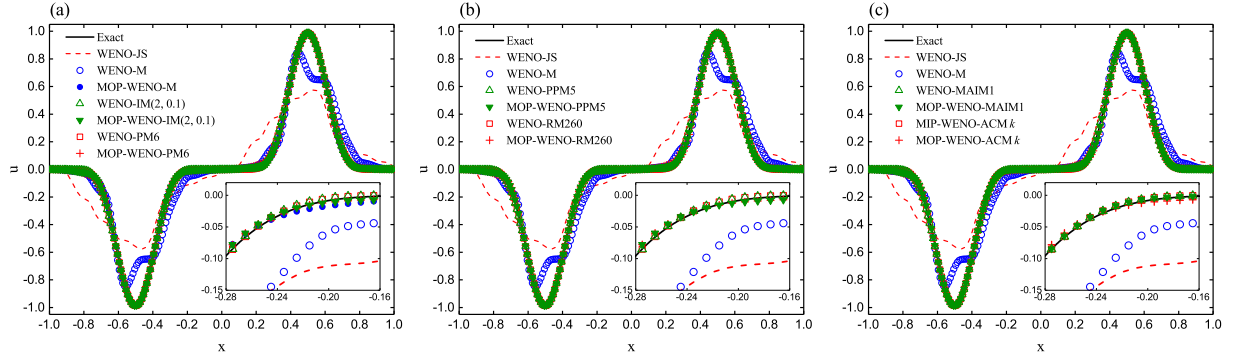


Fig. 2. Performance of various WENO schemes for Example 3 at output time $t = 1000$ with a uniform mesh size of $\Delta x = 1/200$.

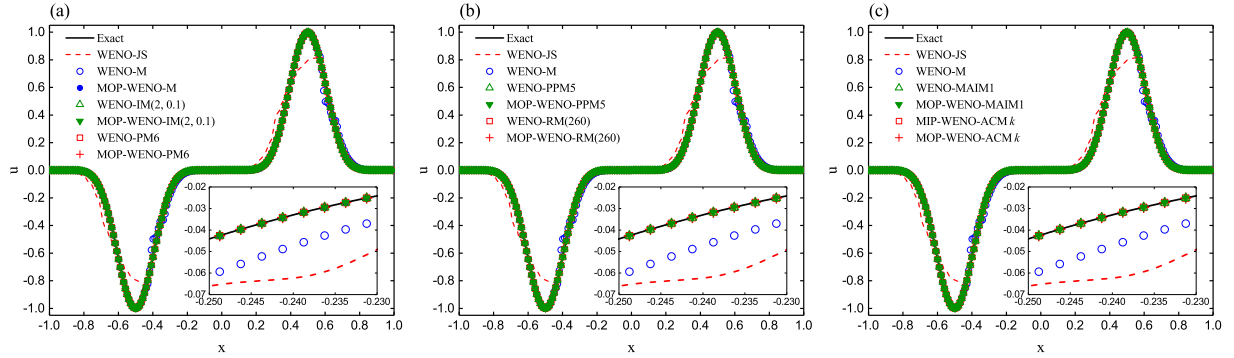


Fig. 3. Performance of various WENO schemes for Example 3 at output time $t = 1000$ with a uniform mesh size of $\Delta x = 1/800$.

Case 2. (BiCWP) The initial condition is given by

$$u(x, 0) = \begin{cases} 0, & x \in [-1.0, -0.8] \cup (-0.2, 0.2] \cup (0.8, 1.0], \\ 0.5, & x \in (-0.6, -0.4] \cup (0.2, 0.4] \cup (0.6, 0.8], \\ 1, & x \in (-0.8, -0.6] \cup (-0.4, -0.2] \cup (0.4, 0.6]. \end{cases} \quad (42)$$

Case 1 and Case 2 were carefully simulated in [18]. Case 1 is called SLP as mentioned earlier in this paper. Case 2 consists of several constant states separated by sharp discontinuities at $x = \pm 0.8, \pm 0.6, \pm 0.4, \pm 0.2$ and it was called BiCWP for brevity in the presentation as the profile of the exact solution for this *Problem* looks like the *Breach in City Wall*.

In Figs. 4, 6 and Figs. 8, 10, we show the comparison of considered schemes for SLP and BiCWP respectively, by taking $t = 2000$ and $N = 800$. It can be seen that: (1) all the MOP-WENO-X schemes produce results with considerable resolutions which are significantly higher than those of the WENO-JS and WENO-M schemes, and what's more, they all do not generate spurious oscillations, while most of their corresponding WENO-X schemes do, when solving both SLP and BiCWP; (2) it should be reminded that the WENO-IM(2, 0.1) scheme appears not to generate spurious oscillations and it gives better resolution than the MOP-WENO-IM(2, 0.1) scheme in most of the region when solving SLP on present computing condition, however, from Fig. 4(b), one can observe that the MOP-WENO-IM(2, 0.1) scheme gives a better resolution of the Gaussian than the WENO-IM(2, 0.1) scheme, and if taking a closer look, one can see that the WENO-IM(2, 0.1) scheme generates a very slight spurious oscillation near $x = -0.435$ as shown in Fig. 4(c); (3) it is very evident as shown in Fig. 8 that, when solving BiCWP, the WENO-IM(2, 0.1) scheme generates the spurious oscillations.

In Figs. 5, 7 and Figs. 9, 11, we show the comparison of considered schemes for SLP and BiCWP respectively,

Table 6. Convergence properties of various considered schemes solving $u_t + u_x = 0$ with initial condition Eq.(41).

N	$t = 2$			$t = 2000$		
	200	400	800	200	400	800
WENO-JS	6.30497e-02(-)	2.81654e-02(1.2103)	1.41364e-02(0.9945)	6.12899e-01(-)	5.99215e-01(0.0326)	5.50158e-01(0.1232)
	1.08621e-01(-)	7.71111e-02(0.4943)	5.69922e-02(0.4362)	5.08726e-01(-)	5.01160e-01(0.0216)	4.67585e-01(0.1000)
	4.09733e-01(-)	4.19594e-01(-0.0343)	4.28463e-01(-0.0302)	7.99265e-01(-)	8.20493e-01(-0.0378)	8.14650e-01(0.0103)
WENO-M	4.77201e-02(-)	2.23407e-02(1.0949)	1.11758e-02(0.9993)	3.81597e-01(-)	3.25323e-01(0.2302)	3.48528e-01(-0.0994)
	9.53073e-02(-)	6.91333e-02(0.4632)	5.09232e-02(0.4411)	3.59205e-01(-)	3.12970e-01(0.1988)	3.24373e-01(-0.0516)
	3.94243e-01(-)	4.05856e-01(-0.0419)	4.16937e-01(-0.0389)	6.89414e-01(-)	6.75473e-01(0.0295)	6.25645e-01(0.1106)
MOP-WENO-M	5.72690e-02(-)	2.72999e-02(1.0689)	1.42908e-02(0.9338)	3.85134e-01(-)	1.74987e-01(1.1381)	6.40251e-02(1.4505)
	1.00827e-01(-)	7.33765e-02(0.4585)	5.57886e-02(0.3953)	3.48164e-01(-)	1.86418e-01(0.9012)	1.07629e-01(0.7925)
	4.14785e-01(-)	4.45144e-01(-0.1019)	4.64024e-01(-0.0599)	7.41230e-01(-)	5.04987e-01(0.5537)	4.81305e-01(0.0693)
WENO-IM(2,0.1)	4.40293e-02(-)	2.02331e-02(1.1217)	1.01805e-02(0.9909)	2.17411e-01(-)	1.12590e-01(0.9493)	5.18367e-02(1.1190)
	9.19118e-02(-)	6.68479e-02(0.4594)	4.95333e-02(0.4325)	2.30000e-01(-)	1.64458e-01(0.4839)	9.98968e-02(0.7192)
	3.86789e-01(-)	3.98769e-01(-0.0441)	4.09515e-01(-0.0383)	5.69864e-01(-)	4.82180e-01(0.2410)	4.73102e-01(0.02784)
MOP-WENO-IM(2,0.1)	6.09985e-02(-)	2.86731e-02(1.0891)	1.45601e-02(0.9777)	3.83289e-01(-)	1.67452e-01(1.1947)	6.44253e-02(1.3780)
	1.03438e-01(-)	7.56598e-02(0.4512)	5.61842e-02(0.4294)	3.47817e-01(-)	1.76550e-01(0.9783)	1.05858e-01(0.7379)
	4.35238e-01(-)	4.62098e-01(-0.0864)	4.64674e-01(-0.0080)	7.25185e-01(-)	5.24538e-01(0.4673)	5.19333e-01(0.0144)
WENO-PM6	4.66681e-02(-)	2.13883e-02(1.1256)	1.06477e-02(1.0063)	2.17323e-01(-)	1.05197e-01(1.0467)	4.47030e-02(1.2347)
	9.45566e-02(-)	6.82948e-02(0.4694)	5.03724e-02(0.4391)	2.28655e-01(-)	1.47518e-01(0.6323)	9.34250e-02(0.6590)
	3.96866e-01(-)	4.06118e-01(-0.0332)	4.15277e-01(-0.0322)	5.63042e-01(-)	5.04977e-01(1.1570)	4.71368e-01(0.0994)
MOP-WENO-PM6	5.45129e-02(-)	2.61755e-02(1.0584)	1.38981e-02(0.9133)	4.51487e-01(-)	1.75875e-01(1.3601)	6.32990e-02(1.4743)
	9.95654e-02(-)	7.16656e-02(0.4744)	5.44733e-02(0.3957)	4.01683e-01(-)	1.83478e-01(1.1305)	1.04688e-01(0.8095)
	4.02785e-01(-)	4.26334e-01(-0.0820)	4.63134e-01(-0.1194)	7.71539e-01(-)	5.06314e-01(0.6077)	4.76091e-01(0.0888)
WENO-PPM5	4.54081e-02(-)	2.07948e-02(1.1267)	1.04018e-02(0.9994)	2.17174e-01(-)	1.03201e-01(1.0734)	4.81637e-02(1.0994)
	9.33165e-02(-)	6.76172e-02(0.4647)	4.99580e-02(0.4367)	2.29008e-01(-)	1.46610e-01(0.6434)	9.47748e-02(0.6294)
	3.91076e-01(-)	4.02214e-01(-0.0405)	4.12113e-01(-0.0351)	5.65575e-01(-)	5.06463e-01(0.1593)	5.14402e-01(-0.0224)
MOP-WENO-PPM5	5.51553e-02(-)	2.65464e-02(1.0550)	1.41381e-02(0.9089)	3.86292e-01(-)	1.75232e-01(1.1404)	6.36336e-02(1.4614)
	9.94592e-02(-)	7.19973e-02(0.4662)	5.52704e-02(0.3814)	3.49072e-01(-)	1.88491e-01(0.8890)	1.06801e-01(0.8196)
	4.04763e-01(-)	4.32887e-01(-0.0969)	4.68577e-01(-0.1143)	7.36405e-01(-)	5.14732e-01(0.5167)	4.98424e-01(0.0464)
WENO-RM(260)	4.63072e-02(-)	2.13545e-02(1.1167)	1.06392e-02(1.0052)	2.17363e-01(-)	1.04347e-01(1.0587)	4.45176e-02(1.2289)
	9.40674e-02(-)	6.81954e-02(0.4640)	5.03289e-02(0.4383)	2.28662e-01(-)	1.47093e-01(0.6365)	9.33066e-02(0.6567)
	3.96762e-01(-)	4.08044e-01(-0.0405)	4.16722e-01(-0.0304)	5.62933e-01(-)	4.98644e-01(0.1750)	4.71450e-01(0.0809)
MOP-WENO-RM(260)	5.54343e-02(-)	2.71415e-02(1.0303)	1.45563e-02(0.8989)	4.56942e-01(-)	2.25420e-01(1.0194)	8.02414e-02(1.4902)
	9.93009e-02(-)	7.22823e-02(0.4582)	5.66845e-02(0.3507)	4.06524e-01(-)	2.25814e-01(0.8482)	1.18512e-01(0.9301)
	4.0041e-01(-)	4.38358e-01(-0.1176)	4.70380e-01(-0.1017)	7.71747e-01(-)	5.12018e-01(0.5919)	4.90610e-01(0.0616)
WENO-MAIMI	5.71142e-02(-)	2.48065e-02(1.2031)	1.21078e-02(1.0348)	2.18238e-01(-)	1.09902e-01(0.9897)	4.41601e-02(1.3154)
	1.03257e-01(-)	7.29236e-02(0.5018)	5.32803e-02(0.4528)	2.29151e-01(-)	1.51024e-01(0.6015)	9.35506e-02(0.6910)
	4.15051e-01(-)	4.23185e-01(-0.0280)	4.28710e-01(-0.0187)	5.63682e-01(-)	4.94657e-01(0.1885)	4.72393e-01(0.0664)
MOP-WENO-MAIMI	5.98640e-02(-)	2.64819e-02(1.1767)	1.33647e-02(0.9866)	2.39900e-01(-)	1.41890e-01(0.7577)	5.43475e-02(1.3845)
	1.05066e-01(-)	7.38102e-02(0.5094)	5.44089e-02(0.4400)	2.47191e-01(-)	1.71855e-01(0.5244)	1.02170e-01(0.7502)
	4.12365e-01(-)	4.26841e-01(-0.0498)	4.38310e-01(-0.0383)	6.06985e-01(-)	5.61908e-01(0.1113)	5.10242e-01(0.1392)
MIP-WENO-ACMk	4.45059e-02(-)	2.03667e-02(1.1278)	1.02183e-02(0.9951)	2.21312e-01(-)	1.10365e-01(1.0038)	4.76589e-02(1.2115)
	9.24356e-02(-)	6.70230e-02(0.4638)	4.96081e-02(0.4341)	2.28433e-01(-)	1.48498e-01(0.6213)	9.40843e-02(0.6584)
	3.92505e-01(-)	4.04024e-01(-0.0417)	4.13511e-01(-0.0335)	5.36242e-01(-)	5.13503e-01(0.0625)	5.15898e-01(-0.0067)
MOP-WENO-ACMk	5.56533e-02(-)	2.79028e-02(0.9961)	1.43891e-02(0.9554)	3.83033e-01(-)	1.77114e-01(1.1128)	6.70535e-02(1.4013)
	9.94223e-02(-)	7.33101e-02(0.4396)	5.51602e-02(0.4104)	3.46814e-01(-)	1.87369e-01(0.8883)	1.09368e-01(0.7767)
	4.03765e-01(-)	4.48412e-01(-0.1513)	4.67036e-01(-0.0587)	7.18464e-01(-)	5.05980e-01(0.5058)	4.80890e-01(0.0734)

by taking $t = 200$ and $N = 3200$. From these solutions computed with larger grid numbers and a reduced but still long output time, it can be seen that: (1) firstly, the WENO-IM(2, 0.1) scheme generates spurious oscillations but the MOP-WENO-IM(2, 0.1) scheme does not while provides an improved resolution when solving SLP; (2) although the resolutions of the results computed by the WENO-JS and WENO-M schemes are significantly improved for both SLP and BiCWP, the MOP-WENO-X schemes still evidently provide much better resolutions; (3) the spurious oscillations generated by the WENO-X schemes appear to be more evident and more intense as the grid number increases, while the corresponding MOP-WENO-X schemes can still avoid spurious oscillations but obtain higher resolutions, when solving both SLP and BiCWP.

For the further interpretation, without loss of generality, in Fig. 12, we present the *non-OP points* of the numerical solutions of SLP computed by the WENO-M and MOP-WENO-M schemes with $N = 800, t = 2000$, and the *non-OP points* of the numerical solutions of BiCWP computed by the WENO-PM6 and MOP-WENO-PM6 schemes with $N = 3200, t = 200$. We can find that there are a great many of *non-OP points* in the solutions of the WENO-M and WENO-PM6 schemes while the numbers of the *non-OP points* in the solutions of the MOP-WENO-M and MOP-WENO-PM6 schemes are zero. Actually, there are many *non-OP points* for all considered mapped WENO-X schemes. And as expected, there are no *non-OP points* for the corresponding MOP-WENO-X schemes and the WENO-JS scheme for all computing cases here. We do not show the results of the *non-OP points* for all computing cases here just for the simplicity of illustration.

In summary, it could be indicated that the general method to introduce the *OP* mapping can help to gain the advantage of achieving high resolutions and in the meantime preventing spurious oscillations when solving problems

with discontinuities for long output times. And this is the most important point we want to report in this paper.

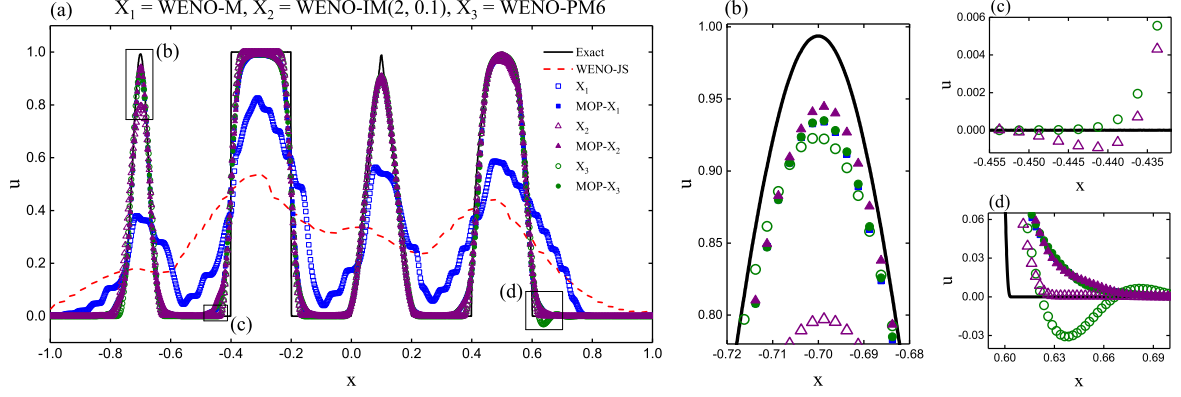


Fig. 4. Performance of the WENO-JS, WENO-M, MOP-WENO-M, WENO-IM(2, 0.1), MOP-WENO-IM(2, 0.1), WENO-PM6 and MOP-WENO-PM6 schemes for the SLP at output time $t = 2000$ with a uniform mesh size of $N = 800$.

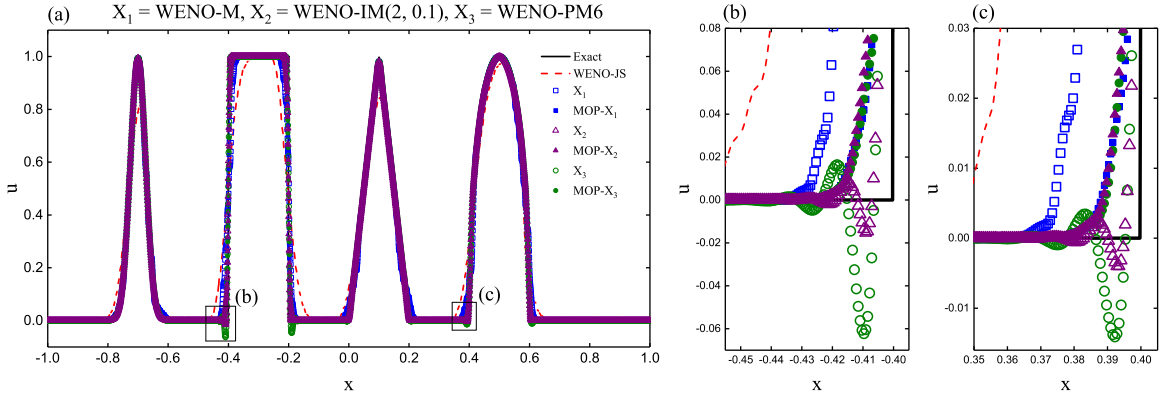


Fig. 5. Performance of the WENO-JS, WENO-M, MOP-WENO-M, WENO-IM(2, 0.1), MOP-WENO-IM(2, 0.1), WENO-PM6 and MOP-WENO-PM6 schemes for the SLP at output time $t = 200$ with a uniform mesh size of $N = 3200$.

4.3. Euler system in two dimension

In this subsection, we focus on the numerical simulations of the shock-vortex interaction problem [2, 20, 22] and the 2D Riemann problem [24, 23, 14]. They are governed by the two-dimensional Euler system of gas dynamics, taking the following strong conservation form of mass, momentum and energy

$$\begin{aligned}
 \frac{\partial \rho}{\partial t} + \frac{\partial(\rho u)}{\partial x} + \frac{\partial(\rho v)}{\partial y} &= 0, \\
 \frac{\partial(\rho u)}{\partial t} + \frac{\partial(\rho u^2 + p)}{\partial x} + \frac{\partial(\rho uv)}{\partial y} &= 0, \\
 \frac{\partial(\rho v)}{\partial t} + \frac{\partial(\rho vu)}{\partial x} + \frac{\partial(\rho v^2 + p)}{\partial y} &= 0, \\
 \frac{\partial E}{\partial t} + \frac{\partial(uE + up)}{\partial x} + \frac{\partial(vE + vp)}{\partial y} &= 0,
 \end{aligned} \tag{43}$$

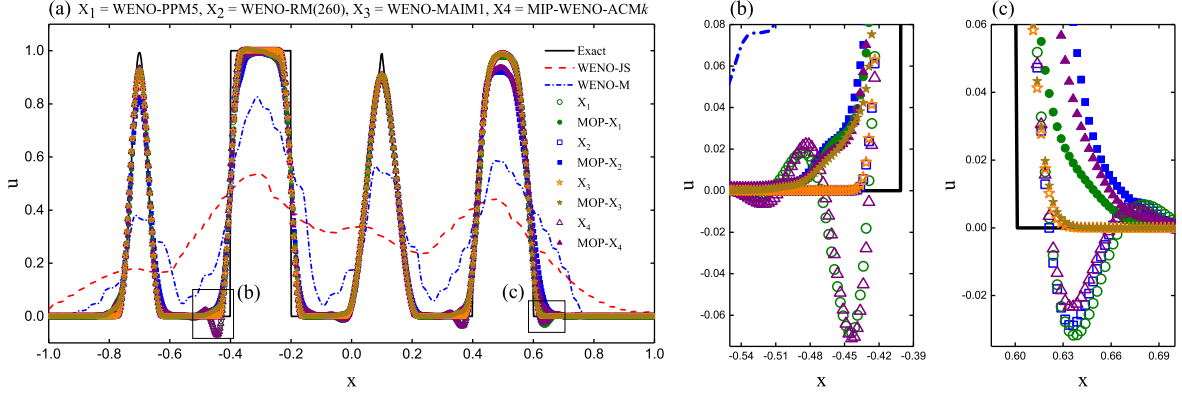


Fig. 6. Performance of the WENO-JS, WENO-M, WENO-PPM5, MOP-WENO-PPM5, WENO-RM260, MOP-WENO-RM260, WENO-MAIM1, MOP-WNEO-MAIM1, MIP-WENO-ACM k and MOP-WENO-ACM k schemes for the SLP at output time $t = 2000$ with a uniform mesh size of $N = 800$.

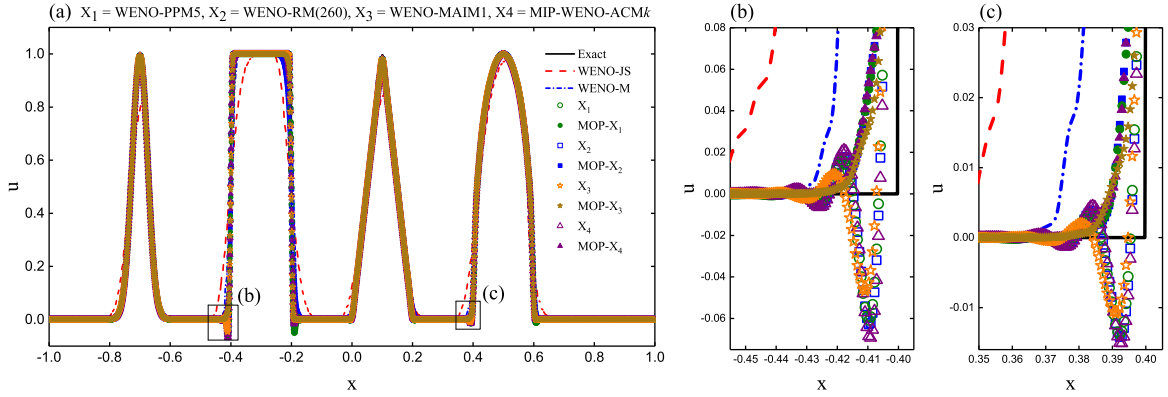


Fig. 7. Performance of the WENO-JS, WENO-M, WENO-PPM5, MOP-WENO-PPM5, WENO-RM260, MOP-WENO-RM260, WENO-MAIM1, MOP-WNEO-MAIM1, MIP-WENO-ACM k and MOP-WENO-ACM k schemes for the SLP at output time $t = 200$ with a uniform mesh size of $N = 3200$.

where ρ, u, v, p and E are the density, components of velocity in the x and y coordinate directions, pressure and total energy, respectively. The following equation of state for an ideal polytropic gas is used to close the two-dimensional Euler system Eq.(43)

$$p = (\gamma - 1)\left(E - \frac{1}{2}\rho(u^2 + v^2)\right),$$

where γ is the ratio of specific heat, and we set $\gamma = 1.4$ in this paper. In the computations below, the CFL number is taken to be 0.5. All the considered WENO schemes are applied dimension-by-dimension to solve the two-dimensional Euler system, and the local characteristic decomposition [13] is used. In [30], Zhang et al. investigated two commonly used classes of finite volume WENO schemes in two dimensional Cartesian meshes, and we employ the one denoted as class A in this subsection.

Example 5. (Shock-vortex interaction) We consider the shock-vortex interaction problem used in [2, 20, 22]. It consists of the interaction of a left moving shock wave with a right moving vortex. The computational domain is initialized by

$$(\rho, u, v, p)(x, y, 0) = \begin{cases} \mathbf{U}_L, & x < 0.5, \\ \mathbf{U}_R, & x \geq 0.5, \end{cases}$$

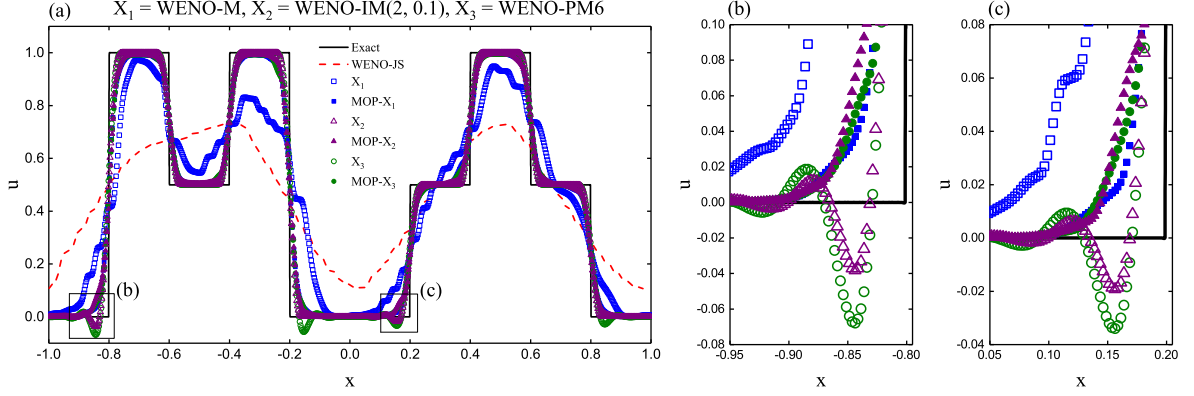


Fig. 8. Performance of the WENO-JS, WENO-M, MOP-WENO-M, WENO-IM(2, 0.1), MOP-WENO-IM(2, 0.1), WENO-PM6 and MOP-WENO-PM6 schemes for the BiCWP at output time $t = 2000$ with a uniform mesh size of $N = 800$.

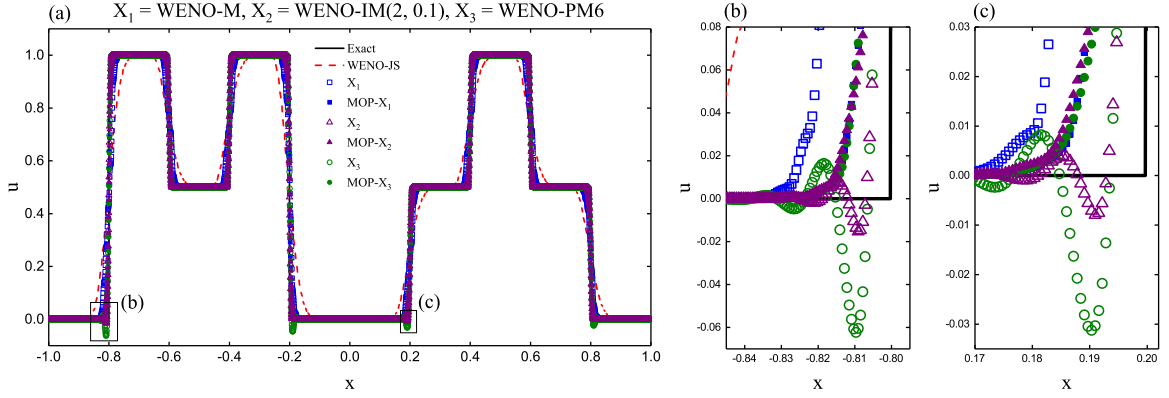


Fig. 9. Performance of the WENO-JS, WENO-M, MOP-WENO-M, WENO-IM(2, 0.1), MOP-WENO-IM(2, 0.1), WENO-PM6 and MOP-WENO-PM6 schemes for the BiCWP at output time $t = 200$ with a uniform mesh size of $N = 3200$.

where $\mathbf{U}_L = (\rho_L, u_L, v_L, p_L) = (1, \sqrt{\gamma}, 0, 1)$, and $\mathbf{U}_R = (\rho_R, u_R, v_R, p_R)$ taking the form

$$\rho_R = 1.3, \rho_R = \rho_L \left(\frac{\gamma - 1 + (\gamma + 1)p_R}{\gamma + 1 + (\gamma - 1)p_R} \right)$$

$$u_R = u_L \left(\frac{1 - p_R}{\sqrt{\gamma - 1 + p_R(\gamma + 1)}} \right), v_R = 0.$$

The vortex $\delta \mathbf{U} = (\delta \rho, \delta u, \delta v, \delta p)$, defined by the following perturbations, is superimposed onto the left state \mathbf{U}_L ,

$$\delta \rho = \frac{\rho_L^2}{(\gamma - 1)p_L} \delta T, \delta u = \epsilon \frac{y - y_c}{r_c} e^{\alpha(1-r^2)}, \delta v = -\epsilon \frac{x - x_c}{r_c} e^{\alpha(1-r^2)}, \delta p = \frac{\gamma \rho_L^2}{(\gamma - 1)p_L} \delta T,$$

where $\epsilon = 0.3, r_c = 0.05, \alpha = 0.204, x_c = 0.25, y_c = 0.5, r = \sqrt{((x - x_c)^2 + (y - y_c)^2)}/r_c^2, \delta T = -(\gamma - 1)\epsilon^2 e^{2\alpha(1-r^2)}/(4\alpha\gamma)$. The transmissive boundary condition is used on all boundaries. A uniform mesh size of 800×800 is used and the output time is set to be $t = 0.35$

We calculate this problem using all the considered mapped WENO-X schemes in Table 1 and their corresponding MOP-WENO-X schemes. For the sake of brevity though, we only present the solutions of the WENO-M, WENO-IM(2, 0.1), WENO-PPM5, WENO-MAIM1 schemes and their corresponding MOP-WENO-X schemes in Figs. 13

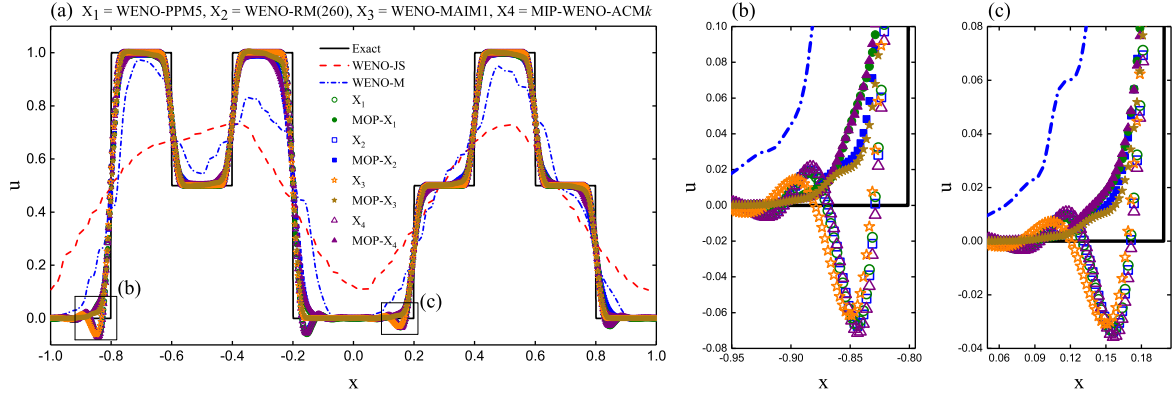


Fig. 10. Performance of the WENO-JS, WENO-M, WENO-PPM5, MOP-WENO-PPM5, WENO-RM260, MOP-WENO-RM260, WENO-MAIM1, MOP-WENO-MAIM1, MIP-WENO-ACM k and MOP-WENO-ACM k schemes for the BiCWP at output time $t = 2000$ with a uniform mesh size of $N = 800$.

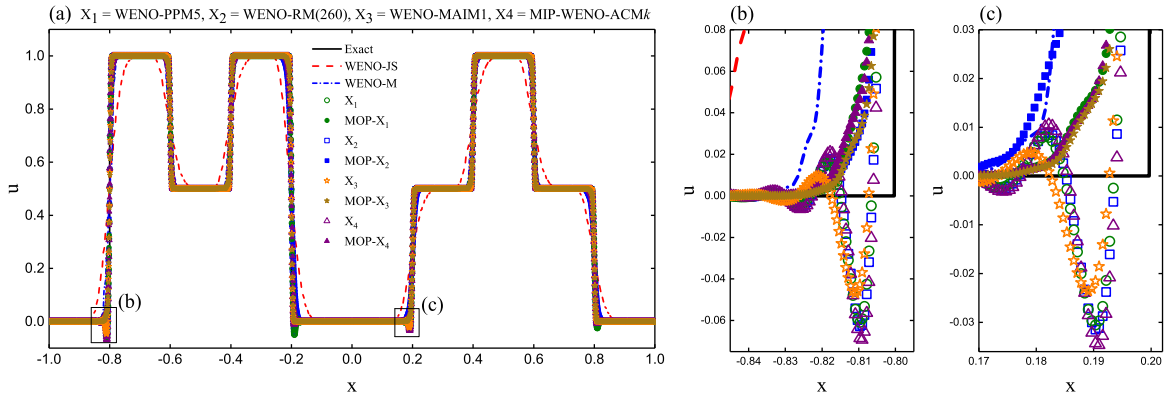


Fig. 11. Performance of the WENO-JS, WENO-M, WENO-PPM5, MOP-WENO-PPM5, WENO-RM260, MOP-WENO-RM260, WENO-MAIM1, MOP-WENO-MAIM1, MIP-WENO-ACM k and MOP-WENO-ACM k schemes for the BiCWP at output time $t = 200$ with a uniform mesh size of $N = 3200$.

and 14, where the first rows give the final structures of the shock and vortex in density profile of the existing mapped WENO-X schemes, the second rows give those of the corresponding MOP-WENO-X schemes, and the third rows give the cross-sectional slices of density plot along the plane $y = 0.65$ where $x \in [0.70, 0.76]$. We find that all the considered schemes perform well in capturing the main structure of the shock and vortex after the interaction. It can be seen that there are clear post-shock oscillations in the solutions of the WENO-M, WENO-IM(2, 0.1) and WENO-PPM5 schemes. However, in the solutions of the MOP-WENO-M, MOP-WENO-IM(2, 0.1) and MOP-WENO-PPM5 schemes, the post-shock oscillations are either removed or significantly reduced. The post-shock oscillations of the WENO-MAIM1 scheme are very slight and even hard to be noticed. Actually, it seems difficult to distinguish the solutions of the WENO-MAIM1 scheme from that of the MOP-WENO-MAIM1 scheme only according to the structure of the shock and vortex in density profile. Nevertheless, when taking a closer look from the cross sectional slices of density profile along the plane $y = 0.65$ at the bottom right picture of Fig. 14 where the reference solution is obtained using the WENO-JS scheme with a uniform mesh size of 1600×1600 , we can see that the post-shock oscillation of the WENO-MAIM1 scheme is very remarkable while it is imperceptible for the MOP-WENO-MAIM1 scheme. Also, from the third rows of Figs. 13 and 14, we find that the WENO-IM(2, 0.1) and WENO-PPM5 schemes generate the post-shock oscillations with much bigger amplitudes than that of the WENO-MAIM1 scheme. The WENO-M scheme also generates clear post-shock oscillations with the amplitudes slightly smaller than that of the

WENO-IM(2, 0.1) and WENO-PPM5 schemes. Evidently, the solutions of the MOP-WENO-M, MOP-WENO-IM(2, 0.1) and MOP-WENO-PPM5 schemes almost generate no post-shock oscillations or only generate some imperceptible numerical oscillations, and their solutions are very close to the reference solution, and this should be an advantage of the mapped WENO schemes whose mapping functions are *OP*.

Example 6. (2D Riemann problem) It is very favorable to test the high resolution numerical methods [14, 15, 21] using the series of 2D Riemann problems [24, 23]. In [14], Lax et al. classified a total of 19 genuinely different Configurations for 2D Riemann problem and calculated all the numerical solutions. The Configuration 4 is chosen here for the test, and the computational domain is initialized by

$$(\rho, u, v, p)(x, y, 0) = \begin{cases} (1.1, 0.0, 0.0, 1.1), & 0.5 \leq x \leq 1.0, 0.5 \leq y \leq 1.0, \\ (0.5065, 0.8939, 0.0, 0.35), & 0.0 \leq x \leq 0.5, 0.5 \leq y \leq 1.0, \\ (1.1, 0.8939, 0.8939, 1.1), & 0.0 \leq x \leq 0.5, 0.0 \leq y \leq 0.5, \\ (0.5065, 0.0, 0.8939, 0.35), & 0.5 \leq x \leq 1.0, 0.0 \leq y \leq 0.5. \end{cases}$$

The transmission boundary condition is used on all boundaries, and the numerical solutions are calculated on a uniform mesh size of 800×800 . The computations proceed to $t = 0.25$.

Similarly, although we calculate this problem using all the considered mapped WENO-X schemes in Table 1 and their corresponding MOP-WENO-X schemes, we only present the solutions of the WENO-M, WENO-PM6, WENO-RM260 and MIP-WENO-ACM k schemes and their corresponding MOP-WENO-X schemes here for the sake of brevity. We have shown the numerical results of density obtained by using these schemes in Figs. 15 and 16, where the first rows give the structures of the 2D Riemann problem in density profile of the existing mapped WENO-X schemes, the second rows give those of the corresponding MOP-WENO-X schemes, and the third rows give the cross-sectional slices of density plot along the plane $y = 0.5$ where $x \in [0.65, 0.692]$. We can see that all schemes can capture the main structure of the solution. However, we can also observe that there are obvious post-shock oscillations (as marked by the pink boxes), which are unfavorable for the fidelity of the results, in the solutions of the WENO-M, WENO-PM6, WENO-RM(260) and MIP-WENO-ACM k schemes. These post-shock oscillations can be seen more clear from the cross-sectional slices of density profile as presented in the third rows of Figs. 15 and 16, where the reference solution is obtained by using the WENO-JS scheme with a uniform mesh size of 3000×3000 . Noticeably, there are either almost no or imperceptible post-shock oscillations in the solutions of the MOP-WENO-M, MOP-WENO-PM6, MOP-WENO-RM(RM260) and MOP-WENO-ACM k schemes. Again, we believe that this should be an advantage of the mapped WENO schemes whose mapping functions are *OP*.

5. Conclusions

We extend the *order-preserving (OP)* mapping introduced in [18] to various existing mapped WENO schemes in references by providing a general formula of their mapping functions. A systematic analysis has been made to prove that the improved mapped WENO scheme based on the existing mapped WENO-X scheme, denoted as MOP-WENO-X, generates numerical solutions with the same convergence rates of accuracy in smooth regions as the corresponding WENO-X scheme. Furthermore, numerical experiments are run to show that the MOP-WENO-X schemes have a same advantage as the mapped WENO scheme proposed in [18] in calculating the one-dimensional linear advection problems including discontinuities with long output times. The mapping functions of the MOP-WENO-X schemes are *OP* and hence able to attain high resolutions and avoid spurious oscillations meanwhile. Moreover, numerical results with the 2D Euler system problems were presented to show that the MOP-WENO-X schemes perform well in simulating the two-dimensional steady problems with strong shock waves to capture the main flow structures and remove or significantly reduce the post-shock oscillations.

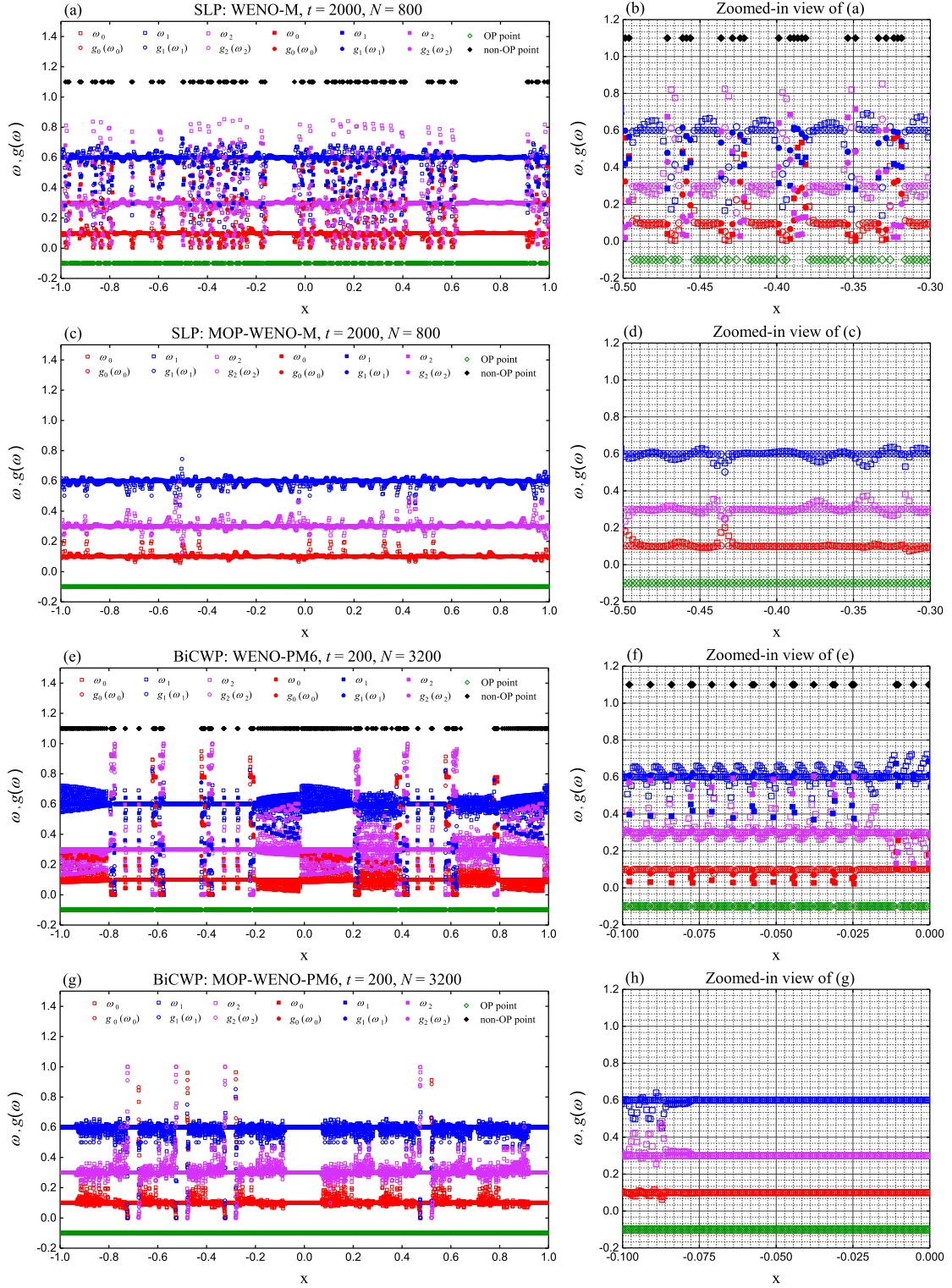


Fig. 12. The *non-OP* points in the numerical solutions of SLP computed by the WENO-M and MOP-WENO-M schemes with $N = 800, t = 2000$, and the *non-OP* points in the numerical solutions of BiCWP computed by the WENO-PM6 and MOP-WENO-PM6 schemes with $N = 3200, t = 200$.

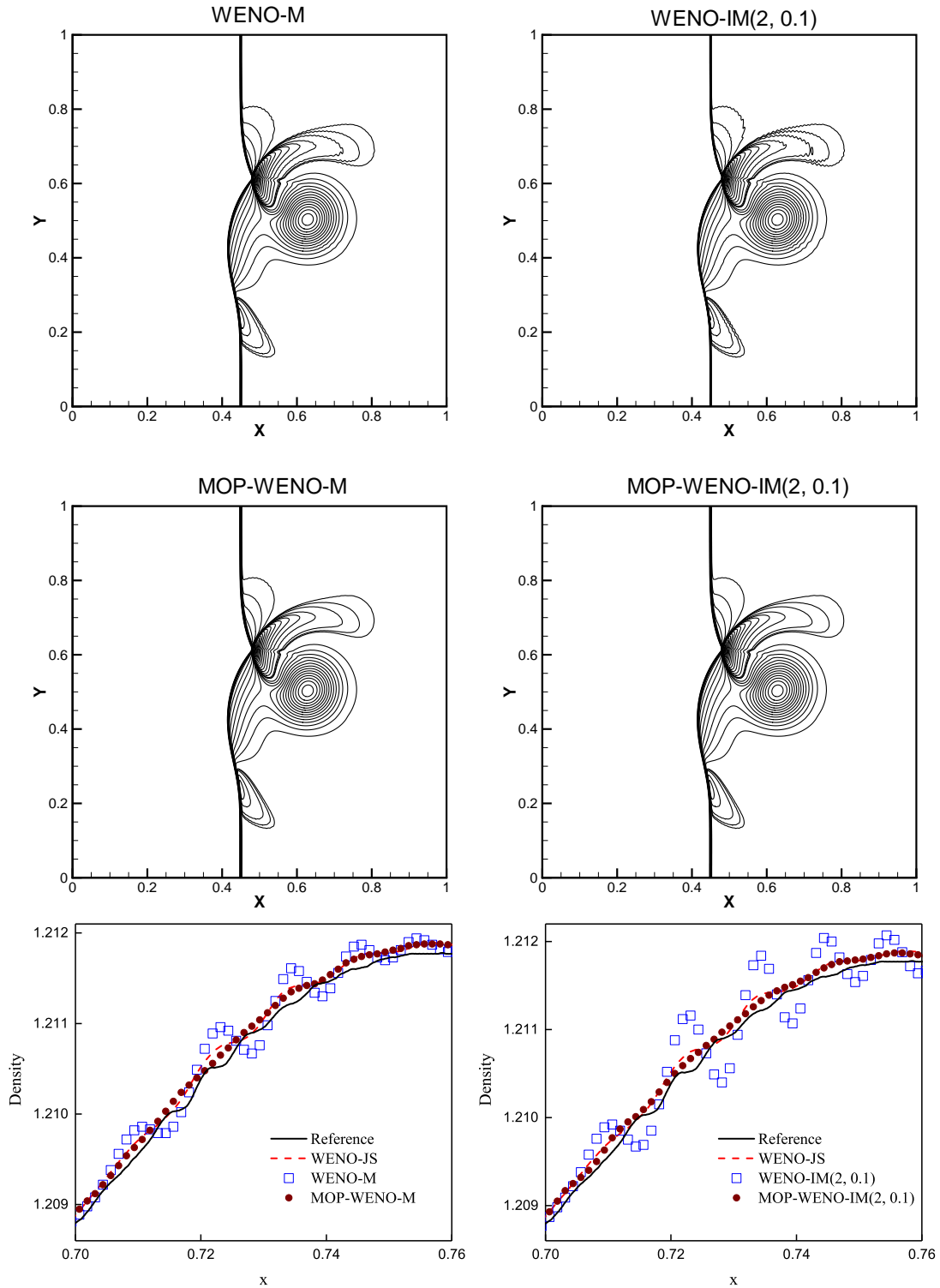


Fig. 13. Density plots for the Shock-vortex interaction using 30 contour lines with range from 0.9 to 1.4 (the first two rows) and the cross-sectional slices of density plot along the plane $y = 0.65$ where $x \in [0.70, 0.76]$ (the third row), computed using the WENO-M and MOP-WENO-M (left column), WENO-IM(2, 0.1) and MOP-WENO-IM(2, 0.1) (right column) schemes.

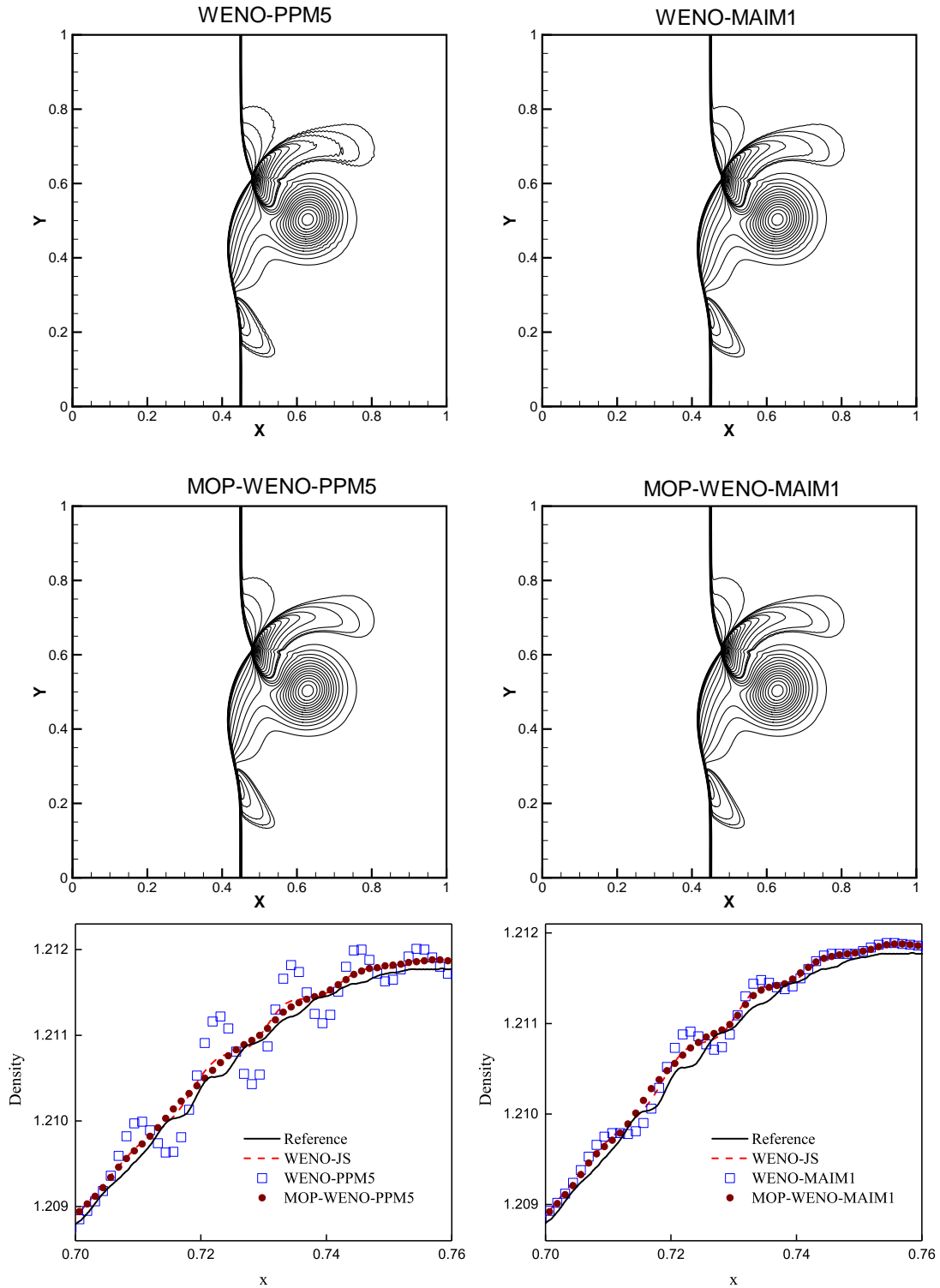


Fig. 14. Density plots for the Shock-vortex interaction using 30 contour lines with range from 0.9 to 1.4 (the first two rows) and the cross-sectional slices of density plot along the plane $y = 0.65$ where $x \in [0.70, 0.76]$ (the third row), computed using the WENO-PPM5 and MOP-WENO-PPM5 (left column), WENO-MAIM1 and MOP-WENO-MAIM1 (right column) schemes.

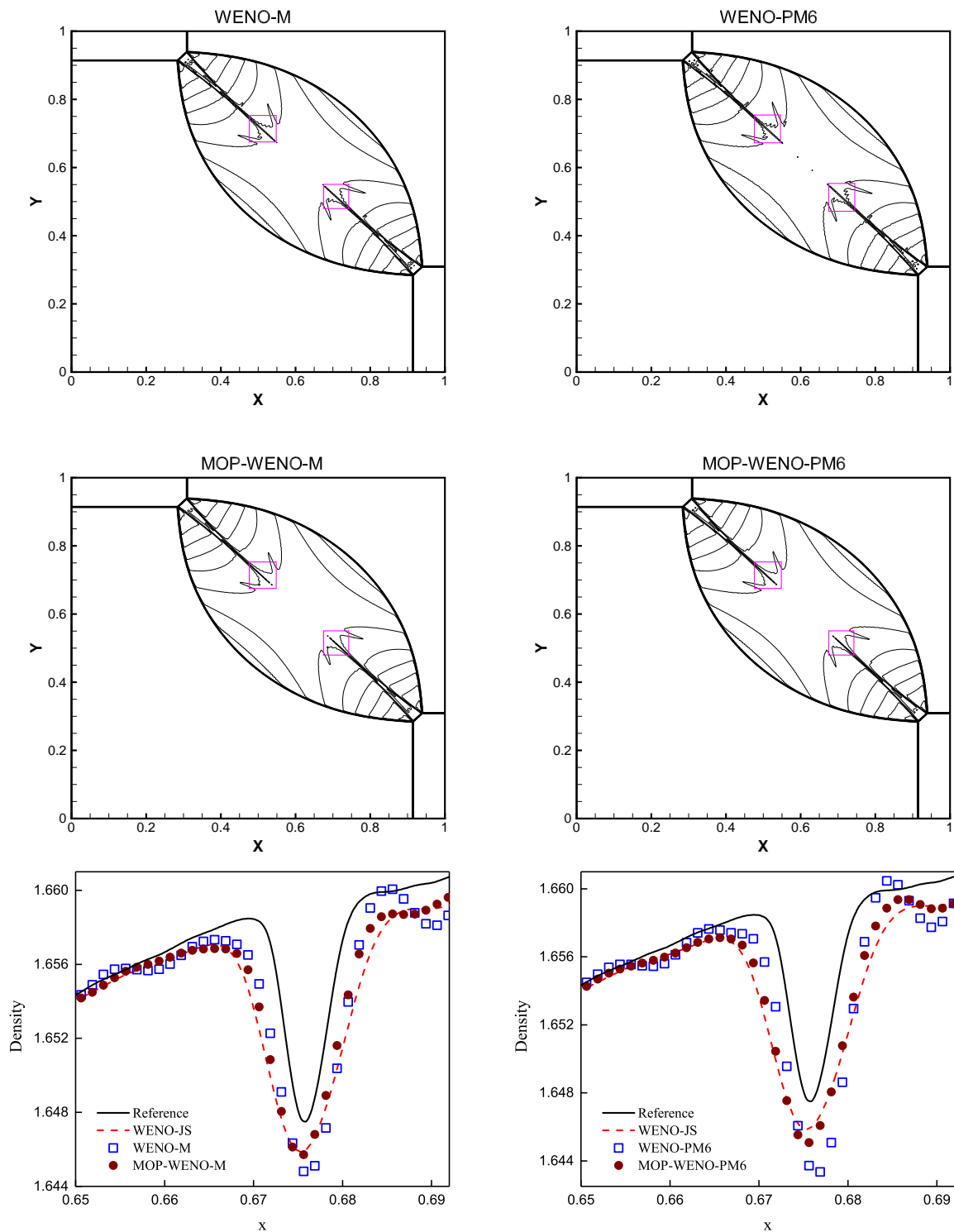


Fig. 15. Density plots for the 2D Riemann problem using 30 contour lines with range from 0.5 to 1.9 (the first two rows) and the cross-sectional slices of density plot along the plane $y = 0.5$ where $x \in [0.65, 0.692]$ (the third row), computed using the WENO-M and MOP-WENO-M (left column), WENO-PM6 and MOP-WENO-PM6 (right column) schemes.

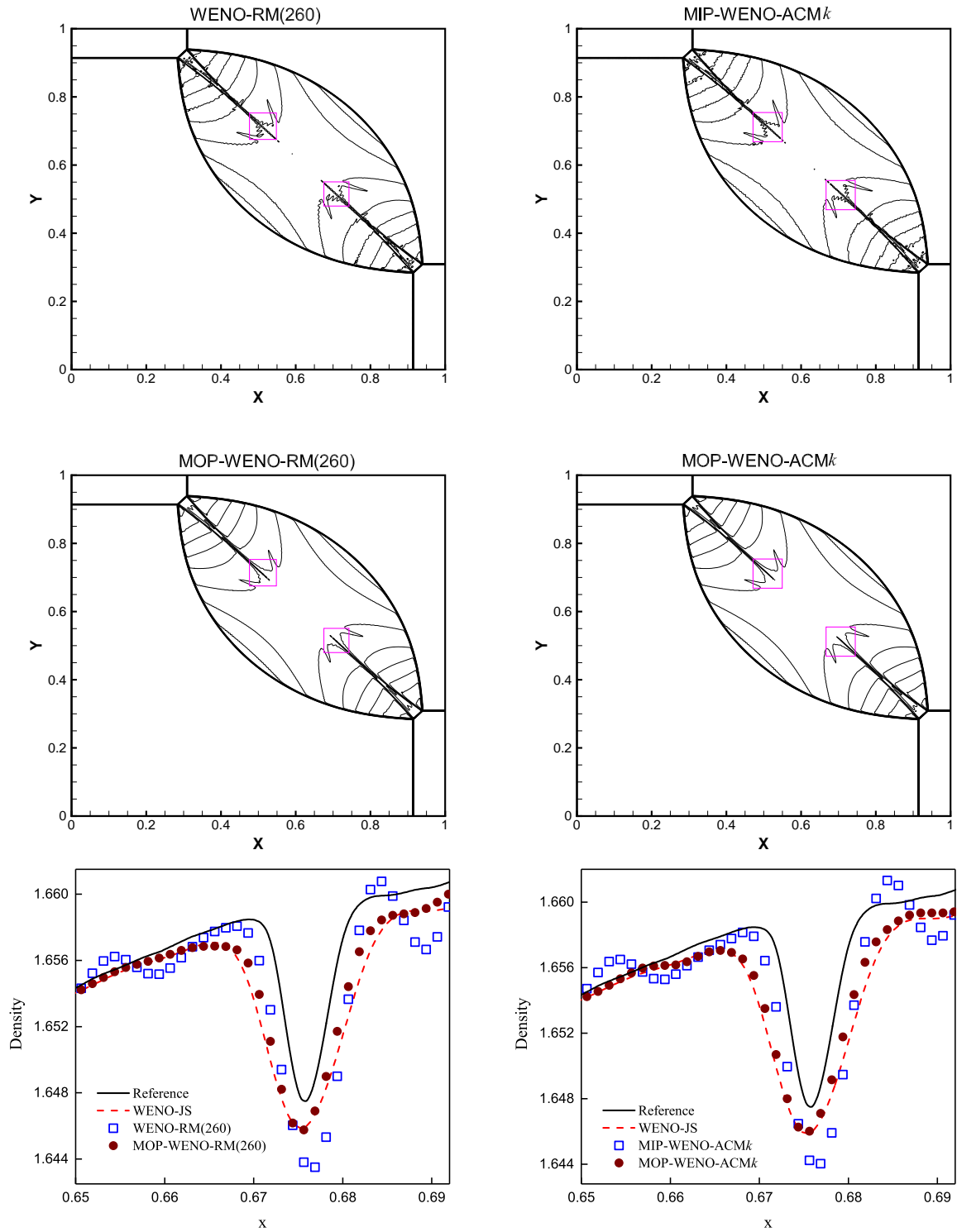


Fig. 16. Density plots for the 2D Riemann problem using 30 contour lines with range from 0.5 to 1.9 (the first two rows) and the cross-sectional slices of density plot along the plane $y = 0.5$ where $x \in [0.65, 0.692]$ (the third row), computed using the WENO-RM(260) and MOP-WENO-RM(260) (left column), MIP-WENO-ACM k and MOP-WENO-ACM k (right column) schemes.

References

- [1] R. Borges, M. Carmona, B. Costa, W.S. Don, An improved weighted essentially non-oscillatory scheme for hyperbolic conservation laws, *J. Comput. Phys.* 227 (2008) 3101–3211.
- [2] A. Chatterjee, Shock wave deformation in shock-vortex interactions, *Shock Waves* 9 (1999) 95–105.
- [3] H. Feng, F. Hu, R. Wang, A new mapped weighted essentially non-oscillatory scheme, *J. Sci. Comput.* 51 (2012) 449–473.
- [4] H. Feng, C. Huang, R. Wang, An improved mapped weighted essentially non-oscillatory scheme, *Appl. Math. Comput.* 232 (2014) 453–468.
- [5] S. Gottlieb, C.W. Shu, Total variation diminishing Runge-Kutta schemes, *Math. Comput.* 67 (1998) 73–85.
- [6] S. Gottlieb, C.W. Shu, E. Tadmor, Strong stability-preserving high-order time discretization methods, *SIAM Rev.* 43 (2001) 89–112.
- [7] A. Harten, ENO schemes with subcell resolution, *J. Comput. Phys.* 83 (1989) 148–184.
- [8] A. Harten, B. Engquist, S. Osher, S.R. Chakravarthy, Uniformly high order accurate essentially non-oscillatory schemes III, *J. Comput. Phys.* 71 (1987) 231–303.
- [9] A. Harten, S. Osher, Uniformly high order accurate essentially non-oscillatory schemes I, *SIAM J. Numer. Anal.* 24 (1987) 279–309.
- [10] A. Harten, S. Osher, B. Engquist, S.R. Chakravarthy, Some results on uniformly high order accurate essentially non-oscillatory schemes, *Appl. Numer. Math.* 2 (1986) 347–377.
- [11] A.K. Henrick, T.D. Aslam, J.M. Powers, Mapped weighted essentially non-oscillatory schemes: Achieving optimal order near critical points, *J. Comput. Phys.* 207 (2005) 542–567.
- [12] G. Hu, R. Li, T. Tang, A robust WENO type finite volume solver for steady Euler equations on unstructured grids, *Commun. Comput. Phys.* 9 (2011) 627–648.
- [13] G.S. Jiang, C.W. Shu, Efficient implementation of weighted ENO schemes, *J. Comput. Phys.* 126 (1996) 202–228.
- [14] P.D. Lax, X.D. Liu, Solution of two-dimensional Riemann problems of gas dynamics by positive schemes, *SIAM J. Sci. Comput.* 19 (1998) 319–340.
- [15] Q. Li, P. Liu, H. Zhang, Piecewise Polynomial Mapping Method and Corresponding WENO Scheme with Improved Resolution, *Commun. Comput. Phys.* 18 (2015) 1417–1444.
- [16] R. Li, W. Zhong, A modified adaptive improved mapped WENO method, arXiv preprint (2020) arXiv:2011.03916.
- [17] R. Li, W. Zhong, An efficient mapped WENO scheme using approximate constant mapping, arXiv preprint (2021) arXiv:2102.00231.
- [18] R. Li, W. Zhong, A new mapped WENO scheme using order-preserving mapping, arXiv preprint (2021) arXiv:2104.04467.
- [19] X.D. Liu, S. Osher, T. Chan, Weighted essentially non-oscillatory schemes, *J. Comput. Phys.* 115 (1994) 200–212.
- [20] S.P. Pao, M.D. Salas, A numerical study of two-dimensional shock-vortex interaction, in: *AIAA 14th Fluid and Plasma Dynamics Conference*, California, Palo Alto, 1981.
- [21] S. Pirozzoli, Numerical methods for high-speed flows, *Annu. Rev. Fluid Mech.* 43 (2011) 163–194.
- [22] Y.X. Ren, M. Liu, H. Zhang, A characteristic-wise hybrid compact-WENO scheme for solving hyperbolic conservation laws, *J. Comput. Phys.* 192 (2003) 365–386.
- [23] C.W. Schulz-Rinne, Classification of the Riemann problem for two-dimensional gas dynamics, *SIAM J. Math. Anal.* 24 (1993) 76–88.
- [24] C.W. Schulz-Rinne, J.P. Collins, H.M. Glaz, Numerical solution of the Riemann problem for two-dimensional gas dynamics, *SIAM J. Sci. Comput.* 14 (1993) 1394–1414.
- [25] C.W. Shu, Essentially non-oscillatory and weighted essentially non-oscillatory schemes for hyperbolic conservation laws, in: *Advanced Numerical Approximation of Nonlinear Hyperbolic Equations. Lecture Notes in Mathematics*, volume 1697, Springer, Berlin, 1998, pp. 325–432.
- [26] C.W. Shu, S. Osher, Efficient implementation of essentially non-oscillatory shock-capturing schemes, *J. Comput. Phys.* 77 (1988) 439–471.
- [27] C.W. Shu, S. Osher, Efficient implementation of essentially non-oscillatory shock-capturing schemes II, *J. Comput. Phys.* 83 (1989) 32–78.
- [28] R. Wang, H. Feng, Observations on the fifth-order WENO method with non-uniform meshes, *Appl. Math. Comput.* 196 (2008) 433–447.
- [29] R. Wang, H. Feng, C. Huang, A New Mapped Weighted Essentially Non-oscillatory Method Using Rational Function, *J. Sci. Comput.* 67 (2016) 540–580.
- [30] R. Zhang, M. Zhang, C.W. Shu, On the order of accuracy and numerical performance of two classes of finite volume WENO schemes, *Commun. Comput. Phys.* 9 (2011) 807–827.
- [31] S. Zhang, C.W. Shu, A new smoothness indicator for the weno schemes and its effect on the convergence to steady state solutions, *J. Sci. Comput.* 31 (2007) 273–305.